





Endothelial Sphingosine-1-Phosphate Receptor 4 Regulates Blood-Brain Barrier Permeability and Promotes a Homeostatic Endothelial Phenotype

 Lena Hansen,¹  Niklas Lohfink,¹ Rajkumar Vutukuri,¹ Roxane-Isabelle Kestner,^{1,3} Sandra Trautmann,⁴ Max Hecht,⁵ Pia Viktoria Wagner,⁵  Daniel Spitzer,^{2,3} Maryam Ibrahim Khel,²  Jadranka Macas,² Nerea Ferreirós,⁴ Robert Gurke,^{4,5} Stefan Günther,⁶ Waltraud Pfeilschifter,^{3*} and Kavi Devraj^{2*}

¹Institute of General Pharmacology and Toxicology, University Hospital, Goethe University Frankfurt, Frankfurt am Main 60528, Germany, ²Institute of Neurology (Edinger Institute), University Hospital, Goethe University Frankfurt, Frankfurt am Main 60528, Germany, ³Department of Neurology, University Hospital, Goethe University Frankfurt, Frankfurt am Main 60528, Germany, ⁴Institute of Clinical Pharmacology, University Hospital, Goethe University Frankfurt, Frankfurt am Main 60528, Germany, ⁵Fraunhofer Institute for Translational Medicine and Pharmacology ITMP, Frankfurt am Main 60596, Germany, and ⁶Max Planck Institute for Heart and Lung Research, Department of Cardiac Development and Remodeling, Bad Nauheim 61231, Germany

The precise regulation of blood-brain barrier (BBB) permeability for immune cells and blood-borne substances is essential to maintain brain homeostasis. Sphingosine-1-phosphate (S1P), a lipid signaling molecule enriched in plasma, is known to affect BBB permeability. Previous studies focused on endothelial S1P receptors 1 and 2, reporting a barrier-protective effect of S1P1 and a barrier-disruptive effect of S1P2. Here, we present novel data characterizing the expression, localization, and function of the S1P receptor 4 (S1P4) on primary brain microvascular endothelial cells (BMECs). Hitherto, the receptor was deemed to be exclusively immune cell associated. We detected a robust expression of S1P4 in homeostatic murine BMECs (MBMECs), bovine BMECs (BBMECs), and porcine BMECs (PBMECs) and pinpointed its localization to abluminal endothelial membranes via immunoblotting of fractionated brain endothelial membrane fragments. Apical S1P treatment of BMECs tightened the endothelial barrier *in vitro*, whereas basolateral S1P treatment led to an increased permeability that correlated with S1P4 downregulation. Likewise, downregulation of S1P4 was observed in mouse brain microvessels (MBMV) after stroke, a neurologic disease associated with BBB impairment. RNA sequencing and qPCR analysis of BMECs suggested the involvement of S1P4 in endothelial homeostasis and barrier function. Using S1P4 knock-out (KO) mice and S1P4 siRNA as well as pharmacological agonists and antagonists of S1P4 both *in vitro* and *in vivo*, we demonstrate an overall barrier-protective function of S1P4. We therefore suggest S1P4 as a novel target regulating BBB permeability and propose its therapeutic potential in CNS diseases associated with BBB dysfunction.

Key words: blood-brain barrier; brain microvascular endothelial cells; endothelial permeability; membrane receptor polarity; sphingosine-1-phosphate receptor 4

Received Jan. 26, 2021; revised Sep. 23, 2021; accepted Sep. 30, 2021.

Author contributions: L.H., R.V., W.P., and K.D. designed research; L.H., N.L., R.V., R.-I.K., S.T., M.H., P.V.W., D.S., M.I.K., J.M., N.F., R.G., S.G., and K.D. performed research; R.-I.K., R.G., S.G., and K.D. contributed unpublished reagents/analytic tools; L.H., N.L., R.V., R.-I.K., M.I.K., R.G., S.G., and K.D. analyzed data; L.H. wrote the first draft of the paper; L.H., R.V., R.-I.K., D.S., S.G., W.P., and K.D. edited the paper; L.H. wrote the paper.

This work was supported by German Research Foundation (DFG) Grants SFB 1039/TP B08 and Z01 and Fondation Leducq Transatlantic Network of Excellence 2014 (SphingoNet). L.H. and R.V. were supported by the Else Kröner-Fresenius-Foundation (EKFS) as part of the Else-Kröner Graduate School. We thank Timothy Hla, Christer Betzholtz, Teresa Sanchez, Josef Pfeilschifter, Richard Proia, Dorothea Schulte, Stefan Liebner, and Robert Brunkhorst for the scientific discussion of S1P4's role at the BBB; Bernhard Brüne and Andreas Weigert

for the donation of global S1P4 KO mice, exchange of knowledge, and continuing scientific discussion; Richard Hawkins for providing luminal and abluminal bovine brain microvascular membrane samples; and the staff of the ZFE (Frankfurt) and mfd Diagnostics (Wendelsheim) animal facilities and Tatjana Starzetz for laboratory technical support.

*W.P. and K.D. contributed equally to this work.

The authors declare no competing financial interests.

Correspondence should be addressed to Waltraud Pfeilschifter at waltraud.pfeilschifter@kgu.de or Kavi Devraj at kavi.devraj@kgu.de.

<https://doi.org/10.1523/JNEUROSCI.0188-21.2021>

Copyright © 2022 the authors

Significance Statement

Many neurologic diseases including multiple sclerosis and stroke are associated with blood-brain barrier (BBB) impairment and disturbed brain homeostasis. Sphingosine-1-phosphate receptors (S1PRs) are potent regulators of endothelial permeability and pharmacological S1PR modulators are already in clinical use. However, the precise role of S1P for BBB permeability regulation and the function of receptors other than S1P1 and S1P2 therein are still unclear. Our study shows both barrier-disruptive and barrier-protective effects of S1P at the BBB that depend on receptor polarization. We demonstrate the expression and novel barrier-protective function of S1P4 in brain endothelial cells and pinpoint its localization to abluminal membranes. Our work may contribute to the development of novel specific S1PR modulators for the treatment of neurologic diseases associated with BBB impairment.

Introduction

Sphingosine-1-phosphate (S1P) is a small phospholipid signaling molecule with numerous cell type-specific functional effects. It is detectable at a high nanomolar to low micromolar concentration in blood plasma, but only at a low nanomolar concentration in the interstitial space of organs (Hla et al., 2008). This physiological gradient between high plasma and low tissue S1P concentrations has been identified as a key chemotactic factor for the egress of lymphocytes from lymph nodes to blood plasma (Schwab et al., 2005). In pathologic conditions associated with endothelial barrier disruption, however, leakage of high plasma S1P concentrations into the interstitial fluid of tissue parenchyma can trigger increased immune cell chemotaxis toward and retention within the inflamed or hypoxic tissue that may aggravate tissue damage (Aoki et al., 2016). The vast majority of the different effects of S1P result from its binding to one of its five membrane-bound G-protein-coupled receptors.

S1P receptor expression at the neurovascular unit is highly cell type-specific. Both murine and human brain microvascular endothelial cells (BMECs) have previously been reported to express S1P receptor 1 (S1P1) and S1P2 (Blaho and Hla, 2014), whereas S1P3 is highly expressed by pericytes and vascular smooth muscle cells (He et al., 2018; Vanlandewijck et al., 2018; VascularSingleCells database, see <http://betsholtzlab.org/VascularSingleCells/database.html>). S1P5 expression is restricted to oligodendrocytes in murine brains, but has been observed in human BMECs (van Doorn et al., 2012). S1P4 expression is generally considered to be immune cell-specific (Olesch et al., 2020) and has not been reported for nonhematopoietic cell types of the neurovascular unit yet.

So far, research on the effects of S1P receptor signaling on vascular endothelial permeability has mainly focused on the opposing effects of S1P1 and S1P2 signaling in lung microvascular endothelial cells. S1P1 activation has been shown to cause a G_i -mediated activation of the small GTPase Rac1 which promotes the formation of cortical actin rings and increases endothelial barrier integrity (Garcia et al., 2001). In contrast, S1P2 signaling in lung endothelial cells is associated with a $G_{12/13}$ -mediated activation of Rho kinase that results in the formation of cytoskeletal actin stress fibers, eventually increasing vascular permeability (Sanchez et al., 2007). With the help of FRET-based biosensors for different G-proteins and GTPases, Reinhard et al. (2017) have confirmed that vascular endothelial permeability is determined by the relative balance between S1P1-mediated G_i and S1P2-mediated $G_{12/13}$ activity. Although substantial knowledge about endothelial S1P1 and S1P2 signaling has been gathered in the past two decades, the precise role of S1P on blood-brain barrier (BBB) regulation

still remains elusive. In this regard, especially the role of S1P receptors other than S1P1 and S1P2 for endothelial permeability is not yet understood.

Novel data acquired via single-cell RNA sequencing indicate a robust expression of S1P4 on all murine BMEC (MBMEC) subtypes (He et al., 2018; Vanlandewijck et al., 2018; VascularSingleCells database, see <http://betsholtzlab.org/VascularSingleCells/database.html>). Our analysis of the above database furthermore pointed toward an EC-specific S1P4 expression at the BBB with no expression by other NVU cell types. It has been reported that S1P4 is able to bind both G_i and $G_{12/13}$ (Gräler et al., 2003), two G-proteins crucial for the control of microvascular endothelial permeability. We thus hypothesized S1P4 to be a possible additional player beside S1P1 and S1P2 that might contribute to the regulation of BBB permeability in homeostasis and/or pathophysiology. Nitzsche et al. (2021) have recently reported an abluminal localization of S1P1 on BMECs. Given the severe functional consequences of S1P gradient loss for endothelial barrier integrity in many pathologic conditions (Hla et al., 2008), we further hypothesized that S1P4 might share this polarization. We thus used a transwell setup that enabled us to conduct polarized S1P treatment experiments either from the apical or the basolateral side of the endothelial monolayer to investigate the role of S1P in BBB permeability regulation and the role of S1P4 receptors therein.

Materials and Methods

Materials

Unless otherwise specified, chemicals were purchased from ROTH (Carl Roth) and reagents from Sigma-Aldrich. Cell culture media, PBS and trypsin-EDTA 1× were from Invitrogen (Thermo Fisher Scientific). Penicillin/streptomycin (10,000 units penicillin and 10-mg streptomycin/ml) and puromycin (10 mg/ml) stock solutions were from Sigma-Aldrich. Ketamine was obtained from Pharmacia & Upjohn, xylazine and buprenorphine from Bayer, and isoflurane from AbbVie Deutschland GmbH. Qubit Assay tubes for cDNA quantification were from Thermo Fisher Scientific.

Growth, purification, and treatment media

Full growth medium (MCDB_{complete}) contained MCDB131 glutamine-free (Invitrogen) supplemented with 20% FBS #7524, 1% glutamin solution 200 mM, 1% Na-heparin solution 1800 units/ml, 1% penicillin/streptomycin (all purchased from Sigma-Aldrich), 1% NaHCO₃ solution 100 mg/ml (ROTH) and 1% ECGS solution (lyophilized porcine brain powder, 5 mg/ml in buffer A). Purification medium (MCDB_{puromycin}) contained 5 μg puromycin/ml MCDB_{complete}. Treatment medium (MCDB_{treatment}) contained MCDB131 glutamine-free (Invitrogen) supplemented with 1% fatty-acid-free BSA, 1% glutamine solution 200 mM and 1% penicillin/streptomycin (all obtained from Sigma-Aldrich).

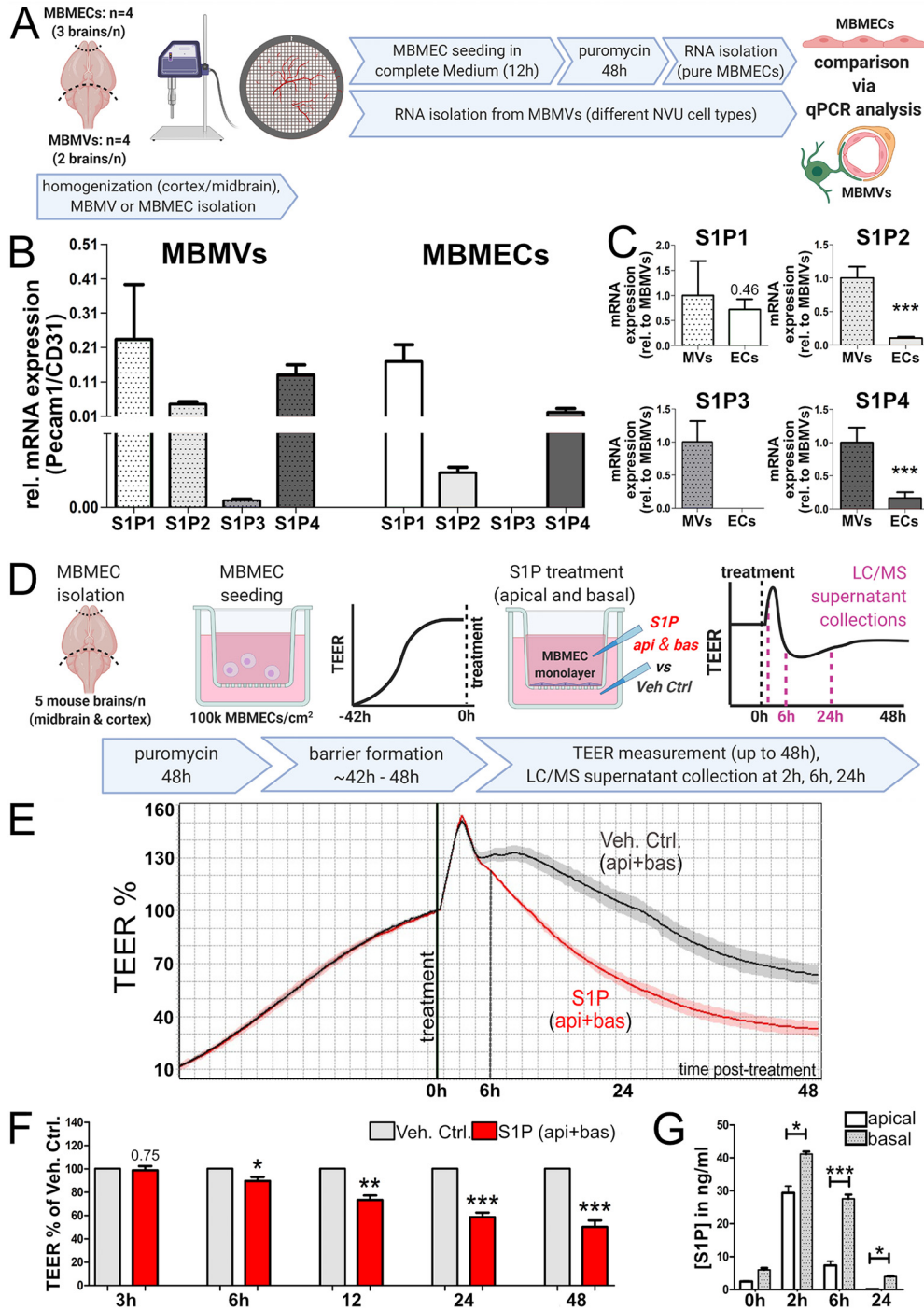


Figure 1. MBMECs express S1P1, S1P2, and S1P4 and react to S1P treatment with a long-term barrier-opening effect that correlates with S1P accumulation at the basal side of the monolayer. **A**, Methodology of MBMEC and MBMV isolation. Both male and female mice (ratio 50:50) were used for brain isolation. **B**, Relative mRNA expression (normalized to Pecam1/CD31) of S1P1–S1P4 in MBMVs and MBMECs, respectively; $n = 4$ each, 2 brains/ n for MBMVs and 3 brains/ n for MBMECs. A scale break was inserted into the y-axis to more clearly resolve the expression of S1P receptors with low transcription levels. **C**, Relative mRNA expression levels (after initial normalization to Pecam1) of each individual S1P receptor in purified MBMEC cultures (ECs) in comparison to freshly isolated MVs. Relative average receptor expression in MVs was set to 1 for better comparability; $n = 4$ (2 brains/ n for MBMVs and 3 brains/ n for MBMECs), statistical significance of receptor expression differences was assessed via two-tailed unpaired Student's t test. Bar graphs represent mean \pm SEM; * indicates significantly altered gene expression levels in MBMECs compared with MBMVs ($***p \leq 0.001$). **D**, Methodology of S1P treatment in a transwell TEER setup. Primary MBMECs (from both sexes, 5 brains/ n) were treated with either 50 nM S1P (TEER) or 100 nM S1P (LC/MS analysis) in a 24-well-transwell insert setup from both apical and basolateral sides. **E**, Representative TEER graph of S1P-treated MBMECs from above experiment. The mean TEER value of three inserts/treatment is shown. **F**, Statistical analysis of the TEER values of MBMECs from above experiment; $n = 5$ (5 mice/ n , both sexes). TEER values after Veh. Ctrl. treatment were set to 100%. Bar graphs represent mean TEER values \pm SEM. Statistical significance between S1P-treated and vehicle control group was assessed for each time point by paired two-tailed Student's t test; * indicates significant TEER differences compared with Veh. Ctrl. treatment, exact p values are specified in the text. **G**, LC/MS analysis of S1P concentrations detected in apical and basal supernatant of MBMECs ($n = 4$ sets of supernatant per compartment and time, 5 mice/ n , both sexes) in a transwell setup after stimulation with 38 ng/ml (100 nM) S1P. Bar graphs represent mean S1P concentrations \pm SEM. Statistical significance between apical and basal S1P concentrations was assessed for each time point by paired two-tailed Student's t test. MBMECs, murine BMECs; MBMVs, mouse brain MVs; TEER, transendothelial electrical resistance.

Isolation of mouse brain microvessels (MBMVs)

MBMVs were isolated as described previously (Gurnik et al., 2016). Briefly, mice were deeply anesthetized (180 mg/kg ketamine and 16 mg/kg xylazine) and transcardially perfused with sterile PBS for 10 min. The isolated brains were stored on ice in MV buffer (MVB: 15 mM HEPES, 5 mM glucose, 147 mM NaCl, 4 mM KCl, 3 mM CaCl₂, 1.2 mM MgCl₂, and 0.5% BSA, pH 7.4). Olfactory lobes, brain stem and cerebellum were removed and the remaining cortex/midbrain segment was rolled on autoclaved Whatman paper (Schleicher & Schuell) to remove the leptomeninges. In case of MBMV isolation post-transient middle cerebral artery occlusion (tMCAO; Fig. 4), ipsilateral and contralateral stroke hemispheres were separated. For MBMV isolation under homeostatic conditions (Figs. 1) both hemispheres were used. Brains were homogenized in MVB with a 0.025-mm clearance glass-Teflon Dounce homogenizer (Wheaton Sciences) propelled by an electric overhead stirrer (VOS14, VWR International) set to 2000 rpm. Myelin fat was removed via density gradient centrifugation in 25% BSA (35 min at 2000 × g), followed by pellet resuspension and filtration through a 100-μm cell strainer (Falcon). For MV recovery, the flow-through was filtered through a 40-μm cell strainer (Falcon). MBMVs were harvested from the nylon meshes for RNA sequencing and qPCR in the respective buffers.

Isolation and purification of primary MBMECs and porcine BMECs (PBMECs)

MBMECs were isolated in a similar fashion to MBMVs as described previously (Gurnik et al., 2016). In short, after the removal of olfactory lobes, brain stem, cerebellum and leptomeninges, brains were stored on ice in buffer A (15 mM HEPES, 153 mM NaCl, 5.6 mM KCl, 1.7 mM CaCl₂, 1.2 mM MgCl₂, and 1% BSA, pH 7.4). Multiple mouse brains were pooled and subsequently homogenized at 2000 rpm with the help of a Dounce homogenizer as described above. The homogenate was digested with 0.75% Collagenase Type II (Worthington) in buffer A (1:1:1 v/v/v, ~3000 U Collagenase II per brain) on a thermo rocker for 1 h at 37°C, 600 rpm. Myelin was removed via density gradient centrifugation with 25% BSA for 35 min at 2000 × g and the remaining cell and vessel pellet was digested in buffer A with collagenase/dispase (Roche; 0.1 U collagenase and 0.8 U dispase per mouse brain) and DNase I (Worthington, 2U DNase per brain) in buffer A on a thermo rocker for 20 min at 37°C, 600 rpm. The cell suspension was centrifuged [400 × g, 4 min, room temperature (TR)] and the pellet was resuspended in MCDB_{complete} medium. PBMEC isolation was done analogous to MBMEC isolation, however pig brain leptomeninges had to be removed manually with surgical pincers. Homogenization was performed on ice at 2000 rpm with a 55 ml Dounce homogenizer (Wheaton Sciences, 0.025-mm clearance) driven by an electric overhead stirrer. Subsequent enzymatic digestions and BSA removal were performed analogous to the MBMEC isolation protocol, however enzyme concentrations were adapted to improve the yield. Collagenase Type II (Worthington) digestion of porcine brain homogenate was performed with 0.75% collagenase Type II solution in buffer A (2:1:2 v/v/v, ~370 U Collagenase II per 1 g of porcine brain tissue). Collagenase/dispase (Roche) digestion was done with 0.01 U collagenase/g, 0.08 U dispase/g, and 0.3 U DNase I (Worthington)/g tissue. After the second enzymatic digestion, the porcine cell and vessel pellet was resuspended in MCDB_{complete} medium. Seeding of murine and porcine cell and MV suspensions in MCDB_{complete} medium was done in six-well plates (two wells per five mouse brains) or T75 cell culture flasks (four flasks per pig brain) precoated with Collagen Type I 150 μg/cm², respectively. BMEC extravasation from MVs and attachment to plate or flask surfaces was allowed for 12 h in MCDB_{complete} before the medium was changed to MCDB_{puromycin} for 48 h to remove nonendothelial cell types. MBMECs were seeded on CellZScope inserts immediately after puromycin treatment. PBMECs were stored deep frozen in liquid nitrogen and seeded on inserts immediately after re-thawing.

Transendothelial electrical resistance (TEER) measurements

One-micrometer pore diameter 24-well PET transwell inserts (Greiner Bio-One) were coated with 5 μg/cm² bovine fibronectin (bnf; Sigma-

Table 1. Murine qPCR primer sequences

Gene	Sense primer (5'→3')	Antisense primer (5'→3')
<i>RPLP0</i>	GTGATGCCAGGGAAGACAGG	GATCTGCTCATCTGCTTGG
<i>Pecam1</i> (CD31)	ATTCCTCAGGCTCGGTCTTC	CCGCCTTCTGTACCTCCTTT
<i>Edg1</i> (S1P1)	CCTTAGCGTTTGCCTGGAGA	CCGATGTCAACTTGCCTGTG
<i>Edg5</i> (S1P2)	CGGCCTTCATCATCTTGT	GGCAGAGTGACATGCCCTGA
<i>Edg3</i> (S1P3)	TGCCTTCTCATAGTATCTT	GGACCAACAGGCAATGAACAC
<i>Edg6</i> (S1P4)	CACGAGTTCCAGCCAGTAG	CTCCACTTCAGCTGCTCTT
<i>Cdh5</i> (VE-Cadherin)	GCCCAGCCTACGAACCTAAA	GGGTGAAGTTGCTGCTCTCGT
<i>Cldn5</i> (Claudin 5)	TGTCGTGCGTGGTGACAGT	TGCTACCCGTGCCTTAACTGG
<i>Ocln</i> (Occludin)	GTGAATGGCAAGCAGCATAACA	TGCCTGAAGCTTCCACACTCA
<i>Tjp1</i> (ZO-1)	TGTTCTCTGCTGGCCCTAA	GGGTGGCTCACTTGGAGTTTC
<i>Rac1</i> (RAC-1)	CAGCTCTCACACAGCGAGGAC	GGCTCCGACATTACACAGCA
<i>RhoA</i> (RHOA)	GGAATGACGAGCACAGGAC	TCCATCTTTGCTTTGCTGAA
<i>Cpm</i> (CPM)	AAGCTTAACCCCGGACGAT	ATTTACAGCAGCAGCTCCA
<i>Cas21</i> (CAS21)	GCAGAAGAGCCCTCAAAGATAA	GAAGCAGGTAGTCCCTCAGA
<i>Id2</i> (ID2)	ACTCGCATCCCACTATCGTCAG	TGCTATCATTTCGACATAAGCTCAGA
<i>Ackr4</i> (CCR11)	AATGCTAGGTGACTCCCATCT	GCCGATTCCAGCATCTGA

Nucleic acid sequences of sense and antisense primers used for qPCR analysis of murine brain MVs and BMEC samples.

Table 2. Porcine qPCR primer sequences

Gene	Sense primer (5'→3')	Antisense primer (5'→3')
<i>RPLP0</i>	GTGATGCCAGGGAAGACAGG	GATCTGCTCATCTGCTTGG
<i>Cdh5</i> (VE-Cadherin)	GGGCGAGTACAGGACACCTT	TCAGTAGCGGAGGTGATG
<i>Rac1</i> (RAC-1)	ATGGGATACGGCTGGACAAGA	CCACAGGATGATGGAGTGT
<i>RhoA</i> (RHOA)	ATCGAGGTGGATGAAAGCAG	GGGCACATTGGGACAGAATG

Nucleic acid sequences of sense and antisense primers used for qPCR analysis of PBMEC samples.

Aldrich) for 90 min before MBMEC/PBMEC seeding. The primary endothelial cells (passage 0) were trypsinized (MBMECs) or thawed (PBMECs), counted and seeded in the bfn-coated transwell inserts (100,000 MBMECs/cm² or 65,000 PBMECs/cm², respectively) in 270 μl MCDB_{complete} medium per insert. TEER was measured and recorded with the aid of a CellZScope device (NanoAnalytics). TEER and Ccl values were obtained from continuous impedance measurements (every 10 min) as described previously (Czupalla et al., 2014). TEER measurements were started immediately after BMEC seeding and the cells remained in MCDB_{complete} medium until barrier formation reached a plateau phase.

Pharmacological treatment

Before pharmacological treatment, all medium in the basal CellZScope compartment and 80% of the medium in the apical compartment was carefully removed (to maintain BMEC monolayer integrity) and exchanged with the appropriate treatment medium. Pharmacological agents were dissolved in fatty acid-free MCDB_{treatment} medium and the appropriate vehicle (or combination of different vehicles) for each agent (or combination of agents) was used to prepare the corresponding control medium. S1P (Tocris) was dissolved in PBS containing 1% fatty acid-free BSA. S1P4 agonist CYM50260 and S1P4 antagonist CYM50358 (both Tocris) were dissolved in DMSO and used at final DMSO concentrations of 1:1000, respectively. Pertussis toxin (Calbiochem) was diluted in PBS and used at a final concentration of 100 ng/ml. The final concentrations of all pharmacological agents used for each experiment are indicated in the corresponding figure legends.

Quantification of TEER measurement data

To compensate slight interinsert TEER differences during barrier formation, TEER values in representative TEER graphs and quantification figures are always shown as percentage of the TEER value measured before treatment (set to 100% for each individual insert). To obtain the electrical resistance values of the cell monolayer, the resistance value of an empty transwell insert was subtracted from each insert's TEER value semi-automatically by NanoAnalytics CellZScope software V.2.2.4.

Table 3. Primary and secondary Western blotting antibodies

Primary antibody	Source	Catalog number	Secondary antibody	Source	Catalog number
Mouse α Pgp (clone C219)	Sigma-Aldrich (Calbiochem)	#517310	IRDye 680RD donkey α mouse	Li-Cor Biosciences	#926-68072
Rabbit α Glut-1	Simpson et al., 2001 (antiserum)	Antiserum	IRDye 800CW donkey α rabbit		#926-32213
Mouse α HSP90 α/β	Santa Cruz	#sc-13119	IRDye 680RD donkey α mouse		#926-68072
			IRDye 800CW donkey α mouse		#926-32212
Mouse α Cldn5 (4C3C2)	Thermo Fisher Scientific	#35-2500	IRDye 680RD donkey α mouse		#926-68072
Goat α VE-Cadherin (C-19)	Santa Cruz	#sc-6458	IRDye 800CW donkey α goat		#926-32214
Rabbit α EDG6 (S1P4)	Thermo Fisher Scientific	#PA5-23221	IRDye 680RD donkey α rabbit		#926-68073
			Goat α rabbit HRP-conjugated	Bio-Rad	#170-6515
Mouse α β -actin	Sigma-Aldrich	#A-2228	Goat α mouse HRP-conjugated		#170-6516

Primary and secondary antibodies used for immunoblot analysis of bovine luminal and abluminal BMEC membrane fragments, MBMECs, and mouse brain homogenate.

TEER values of all individual inserts of the different treatment groups were then normalized to the mean of the corresponding vehicle control values (of the same biological replicate) at each respective time point.

In vitro permeability tracer assay

Permeability tracer assays of pharmacologically treated MBMEC monolayers in transwell inserts were conducted 24 h posttreatment, a time point identified as significant by prior TEER analyses. *In vitro* permeability tracer assays were performed with a multi-size fluorescent dextran tracer mix as described previously (Czupalla et al., 2014). Briefly, different-size dextran tracers [TexasRed-3-kDa dextran (Invitrogen, Thermo Fisher Scientific), tetramethylrhodamine isothiocyanate-20-kDa dextran (Sigma-Aldrich), and fluorescein isothiocyanate-70-kDa dextran (Sigma-Aldrich)] were dissolved in (phenol red-free) DMEM medium (Invitrogen) at a concentration of 2 mM each (= 2 \times tracer mix); 24 h posttreatment, TEER measurements were stopped, and inserts were transferred to a 24-well plate containing 1-ml tracer-free DMEM/well. Half of the top compartment supernatant (135 μ l) was removed from each insert and exchanged with 2 \times tracer mix (final top compartment tracer concentration: 1 mM each). A total of 300 μ l tracer-free DMEM was collected as a control for the subtraction of DMEM background fluorescence. For the next 4 h, every hour, 100- μ l medium was collected from the bottom compartment of each well. At 4 h, medium was also collected from the top compartment as normalization control. Fluorescence intensity of each sample was assessed with the help of a 384-well fluorescence Tecan infinite M200PRO plate reader and i-control 2.0 software (both Tecan) at excitation/emission wavelengths appropriate for all used tracers (595/625 nm for TR, 550/580 nm for TMR, and 490/525 nm for FITC, respectively). Background fluorescence of tracer-free DMEM was subtracted from all measured relative fluorescence unit (RFU) values and the relative fluorescence intensity of bottom chamber supernatant was normalized to the corresponding insert's top compartment fluorescence at 4 h. Inserts with compromised monolayer integrity were excluded from analysis. When comparing different pharmacological treatments and timepoints, the mean fluorescence intensity of the corresponding vehicle control condition at 1 h was set to 100% and the relative fluorescence of all other conditions and timepoints was calculated accordingly.

MBMEC transfection with S1P4 and ctrl siRNA

Primary pure MBMECs (48-h puromycin treatment) were grown to 70% confluency in collagen Type I (150 μ g/cm²)-coated six-well plates and used for transfection with S1P4 siRNA and nontarget control siRNA, respectively. MCDB_{complete} medium was exchanged with MCDB131 (serum-free and antibiotic-free) 2 h before transfection. S1P4 knock-down was performed with RNAi-Mix consisting of four different QIAGEN Flexitube siRNAs (QIAGEN) targeting S1P4 (Mm_Edg6_2, FlexiTube siRNA #SI00989842; Mm_Edg6_3 FlexiTube siRNA #SI00989849; Mm_Edg6_4 FlexiTube siRNA #SI00989856 and Mm_S1pr4_1, FlexiTube siRNA #SI04918536, all 250 nM final). RNAi-Mix and nontarget control siRNA (QIAGEN, siRNA #1022076, 1 μ M final) were used for transfection with RNAiMax lipofectamine (Thermo Fisher Scientific) according to the manufacturer's protocol. Briefly, siRNA oligos (a mix of 4 \times 50

pmol S1P4 siRNAs or 200 pmol Ctrl siRNA, respectively) were pre-diluted in 100 μ l MCDB131 and coincubated with lipofectamine solution (10 μ l RNAiMax lipofectamine pre-diluted in 90 μ l MCDB131) for 15 min at RT before the lipofectamine-siRNA-mix was added to the MBMECs. Six hours posttransfection, MCDB131 was exchanged with MCDB_{complete}, and cells were allowed to recover in full medium overnight. The next morning, MBMECs were trypsinized and cells were seeded on 24-well transwell inserts precoated with 5 μ g/cm² bfn (100,000 MBMECs/cm² in 270 μ l MCDB_{complete}). RNA isolation was performed 48 h posttransfection to ensure that S1P4 knock-down and related gene expression changes were still detectable at the time of harvesting. MBMEC barrier formation on CellZScope inserts was monitored for 96 h posttransfection (when all inserts had reached a TEER value plateau phase eventually).

RNA isolation and reverse transcription

MBMECs/PBMECs were harvested directly from transwell inserts in 350 μ l RLTplus lysis buffer (three inserts/condition/350 μ l RLTplus). RNA was isolated with a RNeasy Plus Microkit (QIAGEN) according to the manufacturer's protocol. Genomic DNA contaminants were digested on microkit columns during RNA isolation. RNA concentrations were measured via QuBit 4 fluorometer (Thermo Fisher Scientific). For RNA sequencing, RNA was frozen immediately after isolation and stored at -80°C until its transfer to the sequencing facility. For qPCR analysis, cDNA was generated from 200 ng RNA/sample using a RevertAid cDNA synthesis kit (Thermo Fisher Scientific) according to the manufacturer's protocol. cDNA was stored frozen at -20°C .

RNA sequencing analysis

RNA was transferred deep frozen (-80°C) to the mRNA sequencing facility at Max Planck Institute for Heart and Lung Research in Bad Nauheim, Germany. RNA quality was verified via LabChip Gx Touch 24 (PerkinElmer). mRNA library preparation with equal amounts of RNA from each sample (100 ng) was achieved with VAHTS Stranded mRNA-seq Library preparation kit (Vazyme) following the manufacturer's protocol. Sequencing was performed with the help of a NextSeq500 Sequencer with 75-bp single-end setup (Illumina). FastQC software (Babraham Bioinformatics) was used to verify signal quality, adaptor content and duplication rate. After adaptor removal and data trimming by Trimmomatic version 0.38, reads of a length between 30 and 150 bp were accepted for further analysis. Trimmed reads were aligned to the murine mm10 genome (Ensembl) with Star 2.7.3a. The maximum ratio of mismatches to mapped length accepted was 10% and reads matching multiple genes or different genomic regions were excluded. The number of reads aligning to genes was counted with featureCounts 1.6.5 tool from the Subread package (Liao et al., 2014). Only reads mapping at least partially inside exons were admitted and aggregated per gene. Reads overlapping multiple genes or aligning to multiple regions were excluded.

TaqMan and SYBR qRT-PCR analysis

TaqMan gene expression assay was used for the comparison of S1P4 expression levels between MBMECs and primary MBMECs (Fig. 1B,C). All other qPCR assays were performed with SYBR Green qRT-PCR. Taqman qPCR was run with an AB7500 fast system (Applied

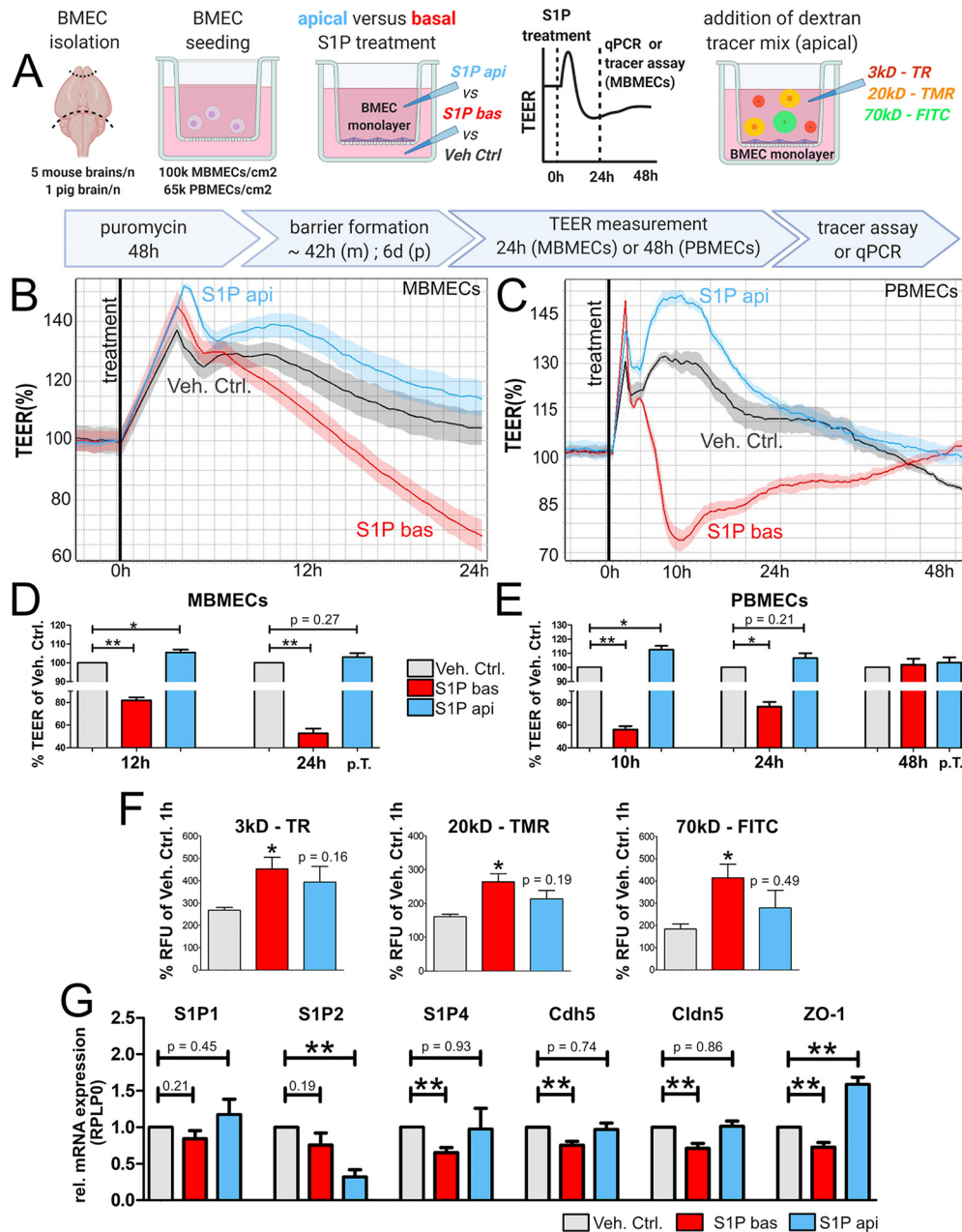


Figure 2. Apical S1P tightens and basal S1P opens primary BMEC barriers. **A**, Methodology of polarized S1P treatment in a transwell TEER setup. Primary MBMECs and PBMECs (brains from both sexes, 5 mouse brains/n or one porcine brain/n, respectively) were treated with 50 nM S1P from either only the apical or only the basolateral side of the monolayer. **B, C**, Representative TEER graphs of the long-term effects of polarized S1P treatment on MBMECs (**B**) and PBMECs (**C**), respectively. The mean of three inserts/condition is shown. **D, E**, Statistical analysis of TEER changes in MBMECs (**D**) or PBMECs (**E**) following polarized S1P treatment compared with vehicle control treatment; $n = 4$ (5 mice/n) for MBMECs and $n = 3$ (1 pig/n) for PBMECs. A scale break was inserted into the y-axis to more clearly resolve the slight yet significant TEER value changes on apical S1P treatment. TEER values after Veh. Ctrl. treatment were set to 100%. Bar graphs represent mean TEER values \pm SEM. Significance between two treatment groups at the same time point was assessed by paired two-tailed Student's *t* test; * indicates significantly different TEER values compared with Veh. Ctrl. treatment, exact *p* values are specified in the text. **F**, Relative fluorescence intensity (RFU) of different-size dextran tracers (TR, 3 kDa; TMR, 20 kDa; and FITC, 70 kDa) in basal supernatant of MBMECs pretreated either with 50 nM apical or 50 nM basal S1P or vehicle control 24 h before permeability assessment. Relative fluorescence 4 h after tracer addition is shown; $n = 4$ (5 mice/n), bar graphs represent mean RFU values \pm SEM. For comparison of two treatment groups, significance was assessed via paired two-tailed Student's *t* test; * indicates significant RFU differences compared with Veh. Ctrl. treatment, exact *p* values are specified in the text. **G**, Relative mRNA expression (normalized to RPLP0) of endothelial S1P receptors, the adherens junction protein VE-Cadherin (*Cdh5*) and the tight junction proteins Claudin 5 (*Cldn5*) and ZO-1 (*Tjp1*) at the 24-h time point after treatment with 50 nM apical or basal S1P compared with vehicle control treatment; $n = 6$ (5 mice/n), the normalized level of gene expression after Veh. Ctrl. treatment was set to 1. Bar graphs represent mean mRNA expression \pm SEM. Significance between two treatment groups was assessed via paired two-tailed Student's *t* test; * indicates significantly altered gene expression levels compared with Veh. Ctrl. treatment, exact *p* values are specified in the text. MBMECs, murine BMECs; PBMECs, porcine BMECs; RFU, relative fluorescence unit; TEER, transendothelial electrical resistance.

Biosystems) qPCR device. Taqman probes [CD31: Mm01242576, S1pr1: Mm02619656, S1pr2: AJVI4VC (customized), S1pr3: Mm02620181 and S1pr4: Mm00468695] were acquired from Life Technologies. Relative mRNA expression levels were calculated using the $2^{-\Delta\Delta CT}$ method. For SYBR qRT-PCR, Absolute SYBR GREEN fluorescein mix (Thermo

Fisher Scientific) was used and RT-PCR was run with a CFX96 Real-Time C1000 thermal cycler. Data were analyzed and relative mRNA expression levels were calculated with Bio-Rad CFX manager Software 3.1 based on the $2^{-\Delta\Delta CT}$ method. The amplification efficiency of murine and porcine qPCR primers was confirmed via relative qPCR standard

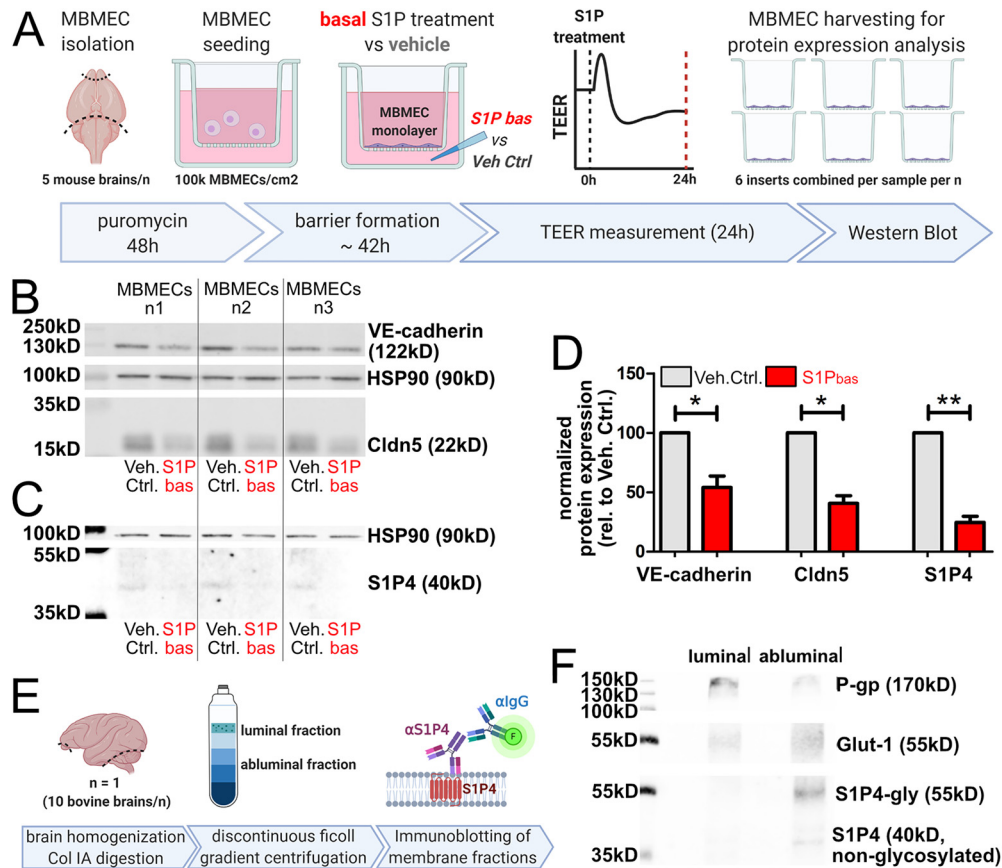


Figure 3. Basolateral S1P treatment is associated with the downregulation of endothelial junction molecules and S1P4, a receptor primarily located on abluminal endothelial membranes. **A**, Methodology of basal S1P treatment in a transwell setup with subsequent protein isolation from the inserts. Primary MBMECs (brains from both sexes, 5 mouse brains/n) were treated with 50 nM S1P or vehicle control from the basolateral side of the monolayer; 24 h posttreatment, cells were harvested and used for Western blot analysis. **B**, Immunoblot staining (20- μ g protein) for VE-Cadherin (VE-Cadh.) and Claudin 5 (Cldn5) in MBMECs from the above experiment ($n = 3$ S1P-treated vs 3 vehicle-treated MBMEC sets, 5 mice/n), HSP90 serves as normalization control. To improve band visibility, contrast and brightness adjustments were applied equally to all pixels of the image. **C**, Immunoblot staining (20- μ g protein) for S1P4 in MBMECs from the above experiment ($n = 3$ S1P-treated vs 3 vehicle-treated MBMEC sets, 5 mice/n), HSP90 serves as normalization control. To improve band visibility, contrast and brightness adjustments were applied equally to all pixels of the image. **D**, Relative protein expression (normalized to HSP90) of VE-Cadherin, Cldn5, and S1P4 in MBMECs 24 h after treatment with 50 nM basal S1P compared with vehicle control treatment; $n = 3$ (5 mice/n), the normalized level of protein expression after Veh. Ctrl. treatment was set to 100%. Bar graphs represent normalized mean protein quantification levels \pm SEM. Significance between two treatment groups was assessed via paired two-tailed Student's *t* test; * indicates significantly altered gene expression levels compared with Veh. Ctrl. treatment, exact *p* values are specified in the text. **E**, Methodology of the isolation process of luminal and abluminal BBMEC membrane fragments and subsequent fluorescent Western blotting of membrane proteins. **F**, Immunoblot staining for S1P4 on luminal and abluminal BBMEC membranes ($n = 1$ from 10 bovine brains). The membrane proteins Pgp and Glut-1 serve as controls. MBMECs, murine BMECs; Col IA, collagenase Type IA; Pgp, permeability glycoprotein 1; Glut1, glucose transporter 1; TEER, transendothelial electrical resistance; HSP90, heat shock protein 90.

curve method before experimental use. Murine qPCR primer sequences are listed in Table 1, porcine qPCR primer sequences in Table 2.

Liquid chromatography–mass spectrometry/mass spectrometry analysis of S1P and S1P4 modulator concentrations in supernatant

After completion of MBMEC barrier formation, MCDB_{complete} medium in both apical and basal compartments of a transwell setup was replaced with MCDB_{treatment} medium containing 38 ng/ml (=100 nM) S1P. A total of 200- μ l supernatant from each compartment were collected 2 h, 6 h and 24 h posttreatment. S1P concentrations in top and bottom supernatants were measured via LC-MS/MS; 200- μ l supernatant sample was mixed with 200- μ l extraction buffer (citric acid 30 mM, disodium hydrogen phosphate 40 mM) and 20- μ l internal standard solution containing sphingosine-d7, sphinganine-d7 (200 ng/ml each), S1P-d7, and sphinganine-1-phosphate-d7 (400 ng/ml each), all from Avanti Polar Lipids. The mixture was extracted once with 1000 μ l methanol/chloroform/hydrochloric acid (15:83:2, v/v/v). After evaporation of the organic phase, reconstitution was performed in 100 μ l tetrahydrofuran/water (9:1, v/v) with 0.2% formic acid and 10 mM ammonium formate. LC-MS/MS analysis applying gradient conditions were performed using an Agilent 1100 LC-system (Agilent Technologies) coupled to an API4000 triple quadrupole MS (Sciex) with a Turbo V Ion Source operating in positive ESI

MRM mode. A Luna C8 column (150 \times 2 mm ID, 3- μ m particle size, 100- Å pore size; Phenomenex) was used. The mobile phases consisted of water with 0.2% formic acid and 2 mM ammonium formate (mobile phase A) and acetonitrile/isopropanol/acetone (50:30:20, v/v/v) with 0.2% formic acid (mobile phase B). Acetonitrile with 0.1% formic acid was infused postcolumn using an isocratic pump at a flow rate of 0.15 ml/min. The internal standard method (isotope dilution mass spectrometry) was employed. Data acquisition and quantification was performed with Analyst software V1.6 and MultiQuant Software V 3.0 (both Sciex).

LC-MS/MS analysis of CYM50260 and CYM50358 was conducted with apical and basal supernatant of MBMECs in a transwell setup collected at 1, 8, and 24 h after basolateral treatment with either CYM50260 or CYM50358, respectively. Here, 20 μ l of supernatant were mixed with 300 μ l 2.5% ammonia in water and 20 μ l internal standard containing 125 ng/ μ l 2,6-dibromo-3-[2,4-dichlorophenoxy] ethoxy-pyridine (Cayman Chemical). The mixture was extracted twice with 500 μ l ethyl acetate. The extracts were combined and evaporated to dryness under a gentle stream of nitrogen at 45°C. The samples were reconstituted in 200 μ l acetonitrile and injected on a Luna C18 150 \times 2.0 mm ID, 3- μ m particle size column (Phenomenex) using a 1200 Infinity Series LC-system (Agilent Technologies). The mobile phase consisted of water +0.1% formic acid (mobile phase A)

and acetonitrile (mobile phase B). An API5500 QTRAP MS (Sciex) in positive ESI MRM mode was used for data acquisition and quantification using Analyst software V1.7.1 and MultiQuant Software V 3.0.2 (both Sciex).

Generation of luminal and abluminal bovine BMEC (BBMEC) membrane fragments

Luminal and abluminal BBMEC membrane fragments were generated as described previously (Devraj et al., 2011). Briefly, MVs were isolated from 10 bovine cortices and digested with collagenase Type IA (1800 units/g) to remove basement membrane, pericytes, and glial fragments. After MV homogenization, luminal and abluminal membrane fractions were separated by discontinuous ficoll gradient centrifugation (as described previously by Sánchez del Pino et al., 1995). BBMEC membrane fragments were stored deep frozen at -80°C and used for Western blot analysis immediately after thawing.

Immunoblotting of BBMEC membrane fragments, MBMECs, and mouse brain homogenate

Total sample protein concentrations were assessed with a BCA assay kit (Thermo Fisher Scientific #23227) according to the manufacturer's protocol. Following sonication, the solubilization of MBMECs and mouse brain homogenate was performed with Laemmli buffer [70 mM Tris-HCl, pH 6.8, 0.6% SDS, 2.5% (w/v) glycerol, 1.25% β -mercaptoethanol, and 0.01% BPB] for 4 min at 94°C . BBMEC membrane fraction samples were solubilized in SB buffer (2.3 M urea, 1.5% SDS, 50 mM Tris, pH 6.8, 25 mM TCEP, and 0.01% BPB) for 1 h at 30°C as described previously (Devraj et al., 2020). Equal amounts of protein were loaded into 10% Tris-HCl bis-acrylamide gels, protein concentrations are mentioned in each blot's corresponding figure legend. For BBMEC membrane immunoblotting, SDS-PAGE was run at a constant 80 V for 3 h and for MBMEC blotting, SDS-PAGE was run at a constant 60 V for 3.5–5 h. For mouse brain homogenate immunoblotting, SDS-PAGE was run at 100 V for 20 min initially, then voltage was increased to 140 V for about 1 h. All SDS-PAGE runs were conducted at room temperature. Proteins were subsequently either transferred to nitrocellulose membranes (Fig. 3B,F) of PVDF membranes (Figs. 3C, 4D). Nitrocellulose blotting was performed at 4°C overnight (36 V constant for 16 h). For blotting on PVDF, membranes were briefly activated with 100% methanol and protein was transferred (70 mA per gel for 1.4 h) at room temperature. Membrane blocking was done with $1\times$ ROTI blocking solution (Carl Roth) for nitrocellulose membranes or 2.5% dry milk in TBST for PVDF membranes, respectively, and antibody stainings were conducted as described previously (Simpson et al., 2001). All used antibodies are listed in Table 3.

MBMEC blots and BBMEC fragment blots were visualized with a LiCOR Odyssey FC Dual Mode Imaging System (Li-COR Biosciences) via use of the 700 nm and 800 m channels, respectively. Mouse brain homogenate blots were visualized after 1 min incubation with enhanced chemiluminescence solution (Pierce ECL Western, Thermo Scientific) and chemiluminescence was detected with light sensitive x-ray film (GE HealthcareHyperfilm ECL, GE Healthcare). To facilitate the detection of S1P4 in brain homogenate despite low protein expression levels, SuperSignal West Femto Maximum Sensitivity Substrate (#34094, Thermo Scientific) was used. Relative protein expression of all blots was determined semi-quantitatively from band densitometry using LiCor ImageStudio version 3.1 software. Quantifications were conducted on raw images. To improve band visibility, brightness and contrast adjustments were subsequently applied uniformly to every pixel of the respective image using Affinity Designer software V.1.8.3.641 (Serif Ltd.). All adjustments were disclosed in the corresponding figure legends.

Animals

Porcine brains for PBMEC isolation were kindly provided by the trauma surgeons of the Goethe University Hospital neuropathology department, Frankfurt am Main (Germany) at the end of a myocardial surgical intervention so that no pigs had to be killed for the purpose of our experiments. C57BL/6J mice were bought from JAX (The Jackson Laboratory) via their European supplier Charles River. Global S1P4 knock-out (KO)

mice were created as described previously (Golfier et al., 2010) and kindly provided to our group by Andreas Weigert and Bernhard Brüne (pathobiochemistry department, Goethe University Hospital). S1P4 KO and C57BL/6J mouse colonies were housed and bred at mfd Diagnostics and transferred to ZFE facility for organ collections and conduct of animal experiments. All animals were kept on a 12/12 h light/dark cycle with food and water *ad libitum*. Before experimental use, S1P4 KO mice were backcrossed to our C57BL/6J strain for 10 generations to minimize transcriptional variation based on genetic background differences. For tMCAO experiments, only male C57BL/6J mice (10 weeks of age) were used, whereas mice of both sexes (10–14 weeks) were used for MBMEC and MBMV isolation and *in vivo* S1P4 antagonist treatment. All animal experiments were conducted in accordance with the German Protection of Animals Act and were approved by the local animal welfare committee (RP Darmstadt, approvals number FU/1143, FU/1014, and FU/1202).

tMCAO

The transient occlusion of the right middle cerebral artery was conducted as described previously (Pfeilschifter et al., 2012). In short, male 10-week-old mice were anesthetized with 1.5% isoflurane under spontaneous respiration with buprenorphine analgesia (0.1 mg/kg). A midline cervical incision was done to expose the right carotid bifurcation and the right common and external carotid arteries were ligated. The middle cerebral artery was occluded for 60 min by advancing a standard silicone rubber-coated monofilament (6–0 medium, Doccol) up to the ostium of the middle cerebral artery. After 1 h, the filament was retracted and reperfusion was allowed. Sham-operated mice received the same surgical intervention, but the silicone filament was retracted immediately. Following the operation, mice were kept on heating mats (Beurer) with jelly food and water access on the cage floor. Animals were killed 24 h post-tMCAO.

In vivo S1P4 antagonist treatment and tracer permeability assay

As no published data about the *in vivo* dosage of the S1P4 antagonist used for this study was available, we based its dosage and the suggested time of application on reference values reported for FTY720 (Czech et al., 2009; Gao et al., 2017) and the TEER kinetics of our own *in vitro* experiments, respectively; 1 mg/kg body weight CYM50358 (Tocris) or the respective DMSO vehicle control was intraperitoneally injected into male and female 10- to 13-week-old wild-type (WT) and S1P4 KO mice twice (16 and 2 h before BBB permeability assessment, respectively). The animals appeared phenotypically normal and showed no signs of pain or neurologic impairment postinjection. *In vivo* BBB permeability tracer assay was performed as described previously (Vutukuri et al., 2018). In short, mice were deeply anesthetized (180 mg/kg ketamine and 16 mg/kg xylazine in 0.9% NaCl solution) and received a lateral tail vein injection with tetramethylrhodamine-conjugated 20-kDa dextran (TMR 20 kDa, Sigma-Aldrich) dissolved in PBS (2 mM TMR tracer, application volume 100 μl). Following 20 min of recirculation, 200- μl cardiac blood was collected from the atrium (normalization control) and mice were transcardially perfused with PBS for 5 min. Brain, lung and kidney were collected and homogenized (one kidney, one hemisphere free of olfactory lobes and cerebellum, or one lobe of the lung in 300- μl PBS, respectively). Following 15 min of centrifugation ($10000\times g$ at 4°C), the fluorescence in organ supernatant and blood serum was measured with a 384-well fluorescence Tecan infinite M200PRO plate reader (Tecan) at 555/585 nm excitation/emission wavelength to assess TMR fluorescence intensity in RFUs. Sham animals (without tracer injection) were used to subtract organ supernatant autofluorescence values. Permeability index (ml/g) at the time points analyzed was calculated as the ratio of (tissue RFUs/g tissue weight) to (serum RFUs/ml serum).

Statistical analyses

Statistical analyses of TEER data, LC-MS/MS data, qPCR, and Western blotting expression data and tracer permeability data were performed using GraphPad Prism 5.0 software (GraphPad Software Inc.); $p < 0.05$ (*) was considered to be statistically significant, as further levels we denoted $p < 0.01$ (**) and $p < 0.001$ (***). Data in graphs are represented

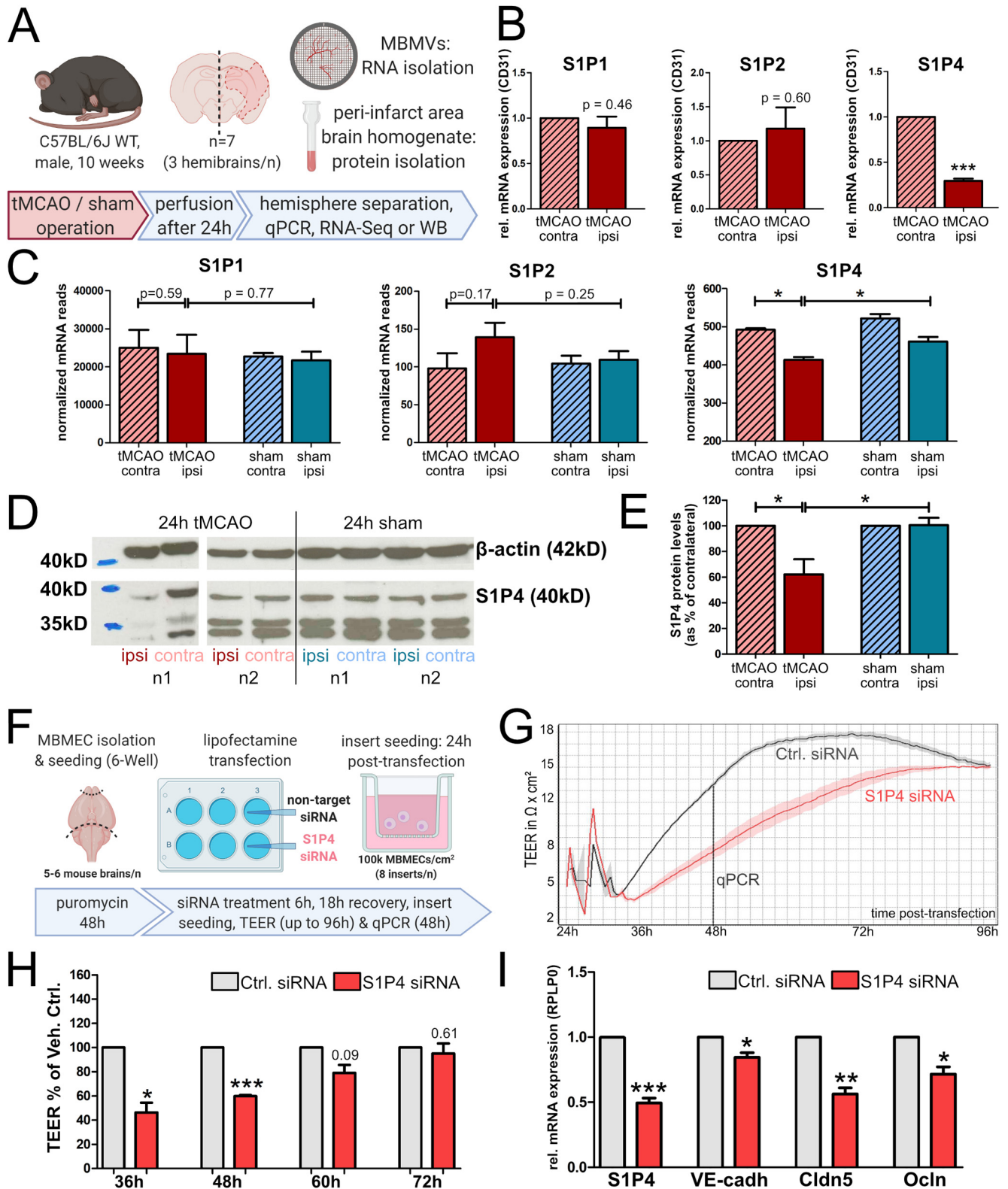


Figure 4. Decreased S1P4 expression is associated with brain microvascular endothelial barrier breakdown. **A**, Methodology of MBMV isolation post-tMCAO for qPCR and RNA sequencing analysis and protein isolation from brain homogenate for Western blot analysis; 24 h post-tMCAO, 10-week-old male mice were transcardially perfused for 10 min to remove immune cells. After ipsilateral and contralateral hemisphere separation, three hemispheres were pooled per n and MBMVs were isolated. For protein isolation, tissue from the peri-infarct area (and the corresponding area of the contralateral hemisphere) of tMCAO- and sham-operated mice was harvested after perfusion. **B**, Relative mRNA expression of the different S1P receptors expressed by MBMECs in ipsilateral and contralateral hemisphere 24 h post-tMCAO; $n = 4$ (3 hemibrains/n), bar graphs represent mean mRNA expression \pm SEM. The normalized level of gene expression in the contralateral hemisphere was set to 1. Statistical significance was assessed by paired two-tailed Student's *t* test; * indicates significantly altered gene expression levels compared with Veh. Ctrl. treatment, exact *p* values are specified in the text. **C**, Normalized mRNA reads of the different endothelial S1P receptors in ipsilateral and contralateral hemispheres of tMCAO-operated and sham-operated mice; $n = 3$, 3 hemibrains/n, bar graphs represent mean mRNA reads \pm SEM. Statistical significance between tMCAO ipsi versus tMCAO contra mRNA reads was assessed by paired two-tailed Student's *t* test. Significance between tMCAO ipsi versus sham ipsi mRNA reads was assessed by unpaired two-tailed Student's *t* test; * indicates significantly altered gene

as mean \pm SEM. The number of animals, cells, biological replicates, and statistical tests employed are described in each experiment's corresponding methodology illustration or figure legend, respectively. Statistical significance of mean S1PR expression level differences between MBMVs and MBMECs as well as between MBMECs from WT and S1P4 KO mice was assessed via unpaired two-tailed Student's *t* test. Statistical significance of TEER and tracer permeability quantifications as well as LC-MS/MS, qPCR, and Western blot analyses of MBMECs that underwent two different pharmacological treatments was assessed via paired two-tailed Student's *t* test. Statistical significance of TEER quantifications and qPCR analysis of S1P4 siRNA-treated and control siRNA-treated MBMECs was assessed via paired two-tailed Student's *t* test. To assess normal distribution of *in vivo* organ permeability index data, D'Agostino and Pearson omnibus normality test was used. Statistical significance of organ permeability index differences between S1P4 antagonist-treated and vehicle-treated mice was thus assessed via Mann-Whitney test for lung permeability indices and via unpaired two-tailed Student's *t* tests for brain and kidney permeability indices. For tMCAO-associated qPCR, RNA sequencing, and Western blot analyses, statistical significance between ipsilateral and contralateral hemispheres (of the same animals) was assessed via paired two-tailed Student's *t* tests, whereas statistical significance between hemispheres from tMCAO-operated and sham-operated animals was assessed via unpaired two-tailed Student's *t* tests. Statistical significance of TEER and tracer permeability quantifications as well as qPCR analyses from MBMECs that received multiple different pharmacological treatments was assessed via ANOVA. For the statistical analysis of RNA sequencing reads, differentially expressed genes were identified using pairwise comparisons with DESeq2 version 1.26.0 (Love et al., 2014). Genes were considered as significantly regulated if a logarithmic fold change of at least \pm 0.585, a mean value higher than 5 and a *p* value lower than 0.05 were reached.

←

expression levels compared with Veh. Ctrl. treatment, exact *p* values are specified in the text. **D**, Representative immunoblot stainings (50- μ g protein, S1P4 signal enhancement with femto substrate) of S1P4 in cortex homogenate from the peri-infarct area and contralateral hemispheres of mice 24 h post-tMCAO (*n* = 2). Cortex homogenate of sham-operated mice (*n* = 2) is shown for comparison, β -actin serves as normalization control. To improve band visibility, contrast and brightness adjustments were applied equally to all pixels of the image. **E**, Relative protein expression (normalized to β -actin) of S1P4 in cortex homogenate of tMCAO-operated and sham-operated mice from the above experiment (*n* = 4 tMCAO, *n* = 3 sham, only the 39-kDa top band of S1P4 was quantified). The normalized level of protein expression in each animal's contralateral hemisphere was set to 100%. Bar graphs represent normalized mean protein quantification levels \pm SEM. Statistical significance between tMCAO ipsi versus tMCAO contra protein expression was assessed by paired two-tailed Student's *t* test. Significance between tMCAO ipsi versus sham ipsi protein expression was assessed by unpaired two-tailed Student's *t* test; * indicates significantly altered gene expression levels compared with Veh. Ctrl. treatment, exact *p* values are specified in the text. **F**, Methodology of S1P4 knock-down in MBMECs. Following S1P4 or control siRNA transfection, cells were seeded on transwell inserts and either used for TEER analysis (up to 96 h post-transfection, 6 inserts/condition/*n*) or harvested for qPCR analysis (48 h posttransfection, 3 inserts/condition/*n*). **G**, Representative TEER graph of delayed MBMEC barrier formation after transfection with S1P4 siRNA compared with nontarget control siRNA. The mean of three inserts/condition is shown. **H**, Statistical analysis of the delayed TEER increase during MBMEC barrier formation following S1P4 knock-down; *n* = 3 (5–6 mice of both sexes/*n*, analysis of 3 inserts/condition/*n*). TEER values after Ctrl. siRNA treatment were set to 100%. Bar graphs represent mean TEER values \pm SEM. Statistical significance between S1P4 knock-down and control treatment was assessed for each time point by paired two-tailed Student's *t* test; * indicates significantly different TEER values compared with Ctrl. siRNA treatment, exact *p* values are specified in the text. **I**, Relative mRNA expression (normalized to RPLP0) of S1P4 and the junctional proteins VE-Cadherin, Cldn5, and Ocln 48 h posttransfection with S1P4 or Ctrl. siRNA; *n* = 4 (5–6 mice/*n*). The normalized level of gene expression after Ctrl siRNA treatment was set to 1, bar graphs represent mean mRNA expression \pm SEM. Statistical significance was assessed by paired two-tailed Student's *t* test; * indicates significantly altered gene expression levels compared with Ctrl. siRNA treatment, exact *p* values are specified in the text. MBMVs, mouse brain MVs, tMCAO, transient cerebral artery occlusion; MBMECs, murine BMECs; TEER, transendothelial electrical resistance.

Graphics software

Methodology illustrations were generated with the help of BioRender. Figures were graphically designed, arranged, and labeled with Affinity Designer software V.1.8.3.641 (Serif Ltd.).

Results

In contrast to apical S1P, basal S1P increases brain microvascular endothelial permeability *in vitro* and leads to transcriptional downregulation of S1P4

Via qPCR-based analysis of S1P receptor expression, we were able to confirm a robust endothelial S1P4 expression both in freshly isolated MBMVs that consist of multiple different NVU cell types and in pure primary MBMECs cultured in puromycin-containing medium for 48 h (Fig. 1A,B). When comparing the relative mRNA expression levels of the different S1P receptors in pure endothelial cells in comparison to MVs (which also contain pericytes, astrocytic endfeet, and vascular smooth muscle cells), we found S1P2 expression to be greatly decreased ($p < 0.0001$, unpaired *t* test; Fig. 1C) and S1P3 not to be expressed at all in pure MBMECs, likely because these two S1P receptors are much more abundantly expressed in pericytes and vascular smooth muscle cells (He et al., 2018; Vanlandewijck et al., 2018; VascularSingleCells database). The relative decrease in S1P4 expression in cultured pure MBMECs in comparison to freshly isolated MVs ($p = 0.0005$, unpaired *t* test) can likely be attributed to immune cell-associated S1P4 expression (Olesch et al., 2020) and/or a possible downregulation of endothelial S1P4 in cell culture (Lyck et al., 2009). In contrast to previous studies using electric cell-substrate impedance sensing (ECIS) devices that only allow apical S1P treatment as MBMECs are seeded directly onto the bottom electrodes in these setups (Garcia et al., 2001; Singleton et al., 2005), we found that S1P treatment of MBMECs (at a low physiological dose of 50 nM) from both sides in a transwell TEER setup (Fig. 1D) only caused a brief, initial tightening effect. This initial tightening is subsequently followed by a long-term barrier opening effect that lasts for >2 d in MBMECs [$p = 0.038$ (6 h), $p = 0.003$ (12 h), $p = 0.0004$ (24 h), and $p = 0.0009$ (48 h), paired *t* tests each; Fig. 1E,F]. LC/MS analysis of S1P concentrations in apical and basal MBMEC supernatants after S1P treatment from both transwell compartments (Fig. 1G) revealed a temporal correlation between the beginning of the barrier-opening phase (about 6 h posttreatment, indicated in Fig. 1E) and a substantial relative accumulation of S1P in the basal compartment at this time point [$p = 0.011$ (2 h), $p < 0.0001$ (6 h), $p = 0.015$ (24 h), paired *t* tests each; Fig. 1G]. In order to verify whether the relative concentration ratio of apical versus basal S1P had an impact on BMEC barrier integrity, we performed polarized S1P treatment experiments with MBMECs and PBMECs in which S1P was added either only from the apical side or only from the basolateral side of the monolayers (Fig. 2A). Statistical significance of mean TEER differences between the three treatment groups (apical S1P, basal S1P, and Veh. Ctrl.) were confirmed via ANOVA ($p < 0.0001$, $F = 107$, $R^2 = 0.96$ for MBMEC TEER values 24 h posttreatment and $p = 0.012$, $F = 10.0$, $R^2 = 0.77$ for PBMEC TEER values 24 h posttreatment). BMECs from both species showed a slight, but significant TEER increase on apical S1P treatment for at least 12 h after treatment [MBMECs: $p = 0.039$ (12-h time point); PBMECs: $p = 0.049$ (10-h time point), paired *t* tests each; Fig. 2B–E] and a much more emphasized, highly significant long-term TEER decrease on basal S1P treatment [MBMECs: $p = 0.006$ (12 h) and $p = 0.002$ (24 h); PBMECs: $p = 0.005$ (10 h) and $p = 0.029$ (24 h), paired *t* tests

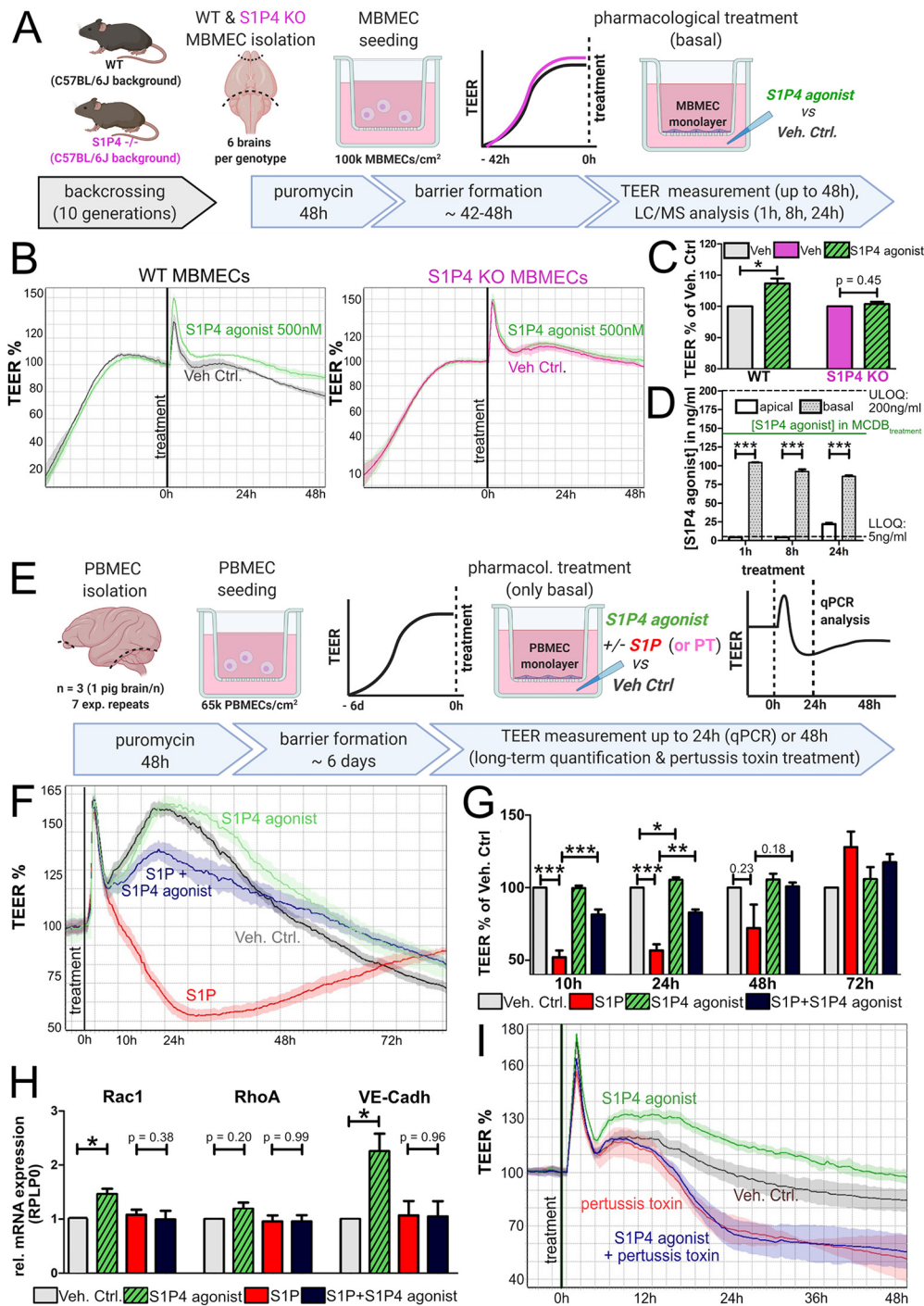


Figure 5. S1P4 agonist tightens BMEC barriers and ameliorates the long-term opening effect of basal S1P. **A**, Methodology. After 10 generations of backcrossing S1P4 KO mice and C57BL/6J WT mice, brains from both male and female mice were used for MBMEC isolation to verify S1P4 agonist specificity ($n = 4$ WT and $n = 3$ KO, 6 brains/n). **B**, Representative TEER graphs of the functional effect of the S1P4 agonist CYM50260 on WT and S1P4 KO MBMECs. S1P4 agonist (500 nM, basal treatment in a transwell setup) has a tightening effect on WT MBMECs, but does not affect S1P4 KO MBMEC barriers. The mean TEER value of three inserts per treatment group ($n = 1$) is shown. **C**, Statistical analysis of TEER values from the above experiment 24 h after S1P4 agonist treatment ($n = 4$ set of WT vs 3 sets of S1P4 KO MBMECs, 6 mice/n). TEER values of three inserts/condition/n were used for analysis. TEER values after Veh. Ctrl. treatment were set to 100% for each genotype. Bar graphs represent mean TEER values \pm SEM. Statistical significance of mean differences between the four groups was confirmed via ANOVA ($p = 0.0006$, $F = 14.36$, $R^2 = 0.81$). Statistical significance between two treatment groups of the same genotype was assessed via paired two-tailed Student's t test; * indicates significantly different mean TEER values between the compared treatment groups, exact p values are specified in the text. **D**, LC/MS analysis of S1P4 agonist concentrations detected in apical and basal supernatant of WT MBMECs ($n = 4$ sets of supernatant per compartment and time, 5 mice/n, both sexes) in a transwell setup 1, 8, and 24 h after basal stimulation with 500 nM S1P4 agonist. Bar graphs represent mean S1P4 agonist concentrations \pm SEM. For at least 8 h poststimulation, S1P4 agonist was undetectable in apical supernatant, indicating barrier impermeability for the compound at early timepoints. Statistical significance between apical and basal S1P concentrations was assessed for each time point by paired two-tailed Student's t test. **E**, Methodology. Basal treatment of PBMECs in a transwell setup (7 experimental repeats with PBMECs from 3 different pigs, 1 male and 2 female) was conducted with 500 nM S1P4 agonist, 20 nM S1P, 20 nM S1P + 500 nM S1P4 agonist and vehicle control medium, respectively. Four sets of PBMECs were harvested 24 h posttreatment for qPCR analysis and three sets of PBMECs were used for 72-h long-term TEER assessment. **F**, Representative TEER graph of the barrier-protective tightening effect of S1P4 agonist on a PBMEC barrier. The mean of three inserts/condition is shown. **G**, Statistical analysis of TEER values from the above experiment; $n = 7$ experimental repeats at 0, 10, and 24 h and $n = 3$ at 48 and 72 h. TEER values of three inserts/condition/n were used for analysis. TEER values

each]. In PBMECs, the maximum barrier-opening effect of basal S1P was reached within 10 h posttreatment and followed by a reversal of the opening effect between 24 h and 48 h (Fig. 2C,E), whereas MBMECs showed a slower, but irreversible barrier opening reaction to basal S1P (Fig. 2B,D). We also verified the long-term barrier-opening effect of basal S1P in MBMECs for larger molecules with permeability assays using fluorescent dextran tracer molecules ranging from 3 to 70 kDa (Fig. 2F). Statistical significance of mean RFU differences (normalized to the top chamber RFU) in MBMEC supernatant after apical S1P, basal S1P and vehicle control treatment was confirmed for 20-kDa-TMR ($p = 0.018$, $F = 6.481$, $R^2 = 0.5902$, ANOVA) and 70-kDa-FITC ($p = 0.045$, $F = 4.70$, $R^2 = 0.54$, ANOVA) tracers. Our analysis indicates a significantly higher permeability of the MBMEC monolayer for all tracer sizes 24 h after basal S1P treatment [$p = 0.02$ (3-kDa-TR), $p = 0.018$ (20 kDa-TMR), and $p = 0.03$ (70-kDa-FITC), paired t tests each]. To gain more insight into the mechanisms underlying this polarized barrier-opening effect of S1P, we isolated mRNA from MBMECs 24 h after S1P or vehicle treatment and conducted a qPCR analysis (Fig. 2G) of all BMEC-associated S1P receptors as well as the adherens junction molecule VE-Cadherin (*Cdh5*) and the tight-junction molecules Claudin 5 (*Cldn5*) and Zona occludens-1 (*Tjp1/ZO-1*). Upon apical S1P treatment, S1P1 and S1P4 mRNA expression remained unaltered in comparison to vehicle control expression, whereas S1P2 expression was significantly decreased ($p = 0.001$, paired t test) and *Tjp1/ZO-1* expression was increased ($p = 0.002$, paired t test). Upon basal S1P treatment, we found a very significant downregulation of all three junctional molecules [$p = 0.006$ (*Cdh5*), $p = 0.009$ (*Cldn5*), $p = 0.008$ (*Tjp1/ZO-1*), paired t tests each]. However, this decrease in barrier-protective gene expression did not correlate with an upregulation of S1P2 or a downregulation of S1P1, but instead with a downregulation of S1P4 ($p = 0.004$, paired t test). To verify the downregulation of S1P4 and endothelial junctional molecules also on protein level, MBMECs were harvested from transwell inserts 24 h after basal S1P or Veh. Ctrl. treatment and protein expression levels were assessed via Western blot analysis (Fig. 3B). In accordance with our qPCR results, we found VE-Cadherin, *Cldn5*, and S1P4

expression to be considerably decreased also on protein level [$p = 0.039$ (VE-Cadherin), $p = 0.012$ (*Cldn5*), and $p = 0.005$ (S1P4), paired t tests each; Fig. 3B–D]. In order to understand whether the significantly altered junctional molecule and S1P receptor expressions observed after basal S1P treatment (Figs. 2G, 3D) could be explained by a polarized localization pattern of S1P4, we performed immunoblotting of luminal and abluminal BBMEC membrane fragments (Fig. 3E). Our analysis strongly indicates the primarily abluminal localization of S1P4 on BMECs (Fig. 3F).

Endothelial S1P4 has an impact on BMEC barrier integrity

We formulated a preliminary hypothesis that the transcriptional downregulation of S1P4 on BMECs might correlate with decreased barrier integrity and thus analyzed the expression of the different endothelial S1P receptors in MBMV's and brain homogenate of mice under conditions of a massive BBB breakdown in the tMCAO stroke model (Fig. 4A). Indeed, we observed a highly significant transcriptional downregulation of S1P4 in MBMV's isolated from the stroke hemisphere of mice 24 h post-tMCAO ($p < 0.0001$, $t = 28.09$, $df = 3$, paired t test; Fig. 4B), whereas S1P1 and S1P2 expression did not significantly differ between stroke and contralateral hemisphere MV's. RNA sequencing data from another set of stroke versus sham MBMV's (Fig. 4C) further revealed that the significant downregulation of S1P4 in the stroke hemisphere did not only occur in comparison to the contralateral hemisphere, but also in comparison to the ipsilateral hemisphere of sham-operated mice [$p = 0.019$ (ipsi tMCAO vs contra tMCAO), $t = 7.150$, $df = 2$, paired t test; $p = 0.029$ (ipsi tMCAO vs ipsi sham), $t = 3.320$, $df = 4$, unpaired t test; RNA sequencing dataset from Kestner et al., 2020, the full dataset is publicly available at GEO, record GSE131193]. The downregulation of S1P4 in the ipsilateral stroke hemisphere 24 h post-tMCAO could also be confirmed on protein level via Western blot analysis of mouse brain homogenate (Fig. 4D,E). The antibody produced three bands at 39, 34, and 32 kDa (Fig. 4D); however, only the top 39-kDa band was used for quantification as we presume the smaller bands to be cleavage products derived from S1P4 degradation or nonspecific bands. Statistical significance of mean S1P4 protein expression differences in cortex homogenate from ipsilateral and contralateral brain hemispheres 24 h after tMCAO or sham operations was confirmed via ANOVA ($p = 0.007$, $F = 7.350$, $R^2 = 0.6880$). In accordance with the previously observed S1P4 downregulation on mRNA level, S1P4 protein expression in cortex homogenate of the ipsilateral stroke hemisphere was likewise significantly decreased (Fig. 4E), both in comparison to the contralateral hemisphere ($p = 0.049$, paired t test) and in comparison to the ipsilateral hemisphere of sham-operated mice ($p = 0.048$, unpaired t test).

Intrigued by these findings, we next investigated whether the increased endothelial permeability in stroke and after basal S1P treatment might be causally connected to the observed S1P4 downregulation in these conditions. To this end, we performed a knock-down of S1P4 in primary MBMECs with siRNA. Unfortunately, the lipofectamine used for siRNA transfection already resulted in a barrier breakdown on its own and thus prevented functional TEER experiments with already-established barriers. We therefore used a different transfection protocol where the cells were transfected first followed by plating on inserts. This protocol with primary MBMECs allowed us to monitor the initial barrier formation following S1P4 and nontarget control siRNA treatment (Fig. 4F). We observed a significantly delayed MBMEC barrier formation after S1P4 knock-

←

after Veh. Ctrl. treatment were set to 100%. Bar graphs represent mean TEER values \pm SEM. Statistical significance of mean differences between the four treatment groups was confirmed via ANOVA for the 10 h ($p < 0.0001$, $F = 56.55$, $R^2 = 0.88$) and 24-h timepoints ($p < 0.0001$, $F = 75.43$, $R^2 = 0.90$). Statistical significance between two treatment groups at the same time point was assessed via paired two-tailed Student's t test; * indicates significantly different mean TEER values between the compared treatment groups, exact p values are specified in the text. **H**, Relative mRNA expression (normalized to RPLP0) of Rac1, RhoA and VE-Cadherin in PBMECs from the above experiment 24 h posttreatment; $n = 4$ experimental repeats (from 2 female and 1 male pigs), the normalized level of gene expression after Veh. Ctrl. treatment was set to 1. Bar graphs represent mean mRNA expression \pm SEM. Statistical significance of mean mRNA expression differences between the four treatment groups were confirmed via ANOVA for Rac1 ($p = 0.02$, $F = 4.51$, $R^2 = 0.53$) and VE-Cadherin ($p = 0.011$, $F = 5.80$, $R^2 = 0.59$). For comparison between two treatment groups, statistical significance was assessed by paired two-tailed Student's t test; * indicates significantly different mRNA expression levels between the compared treatment groups, exact p values are specified in the text. **I**, TEER graph of PBMECs ($n = 1$, 1 male pig, proof-of-principle experiment) after basolateral treatment with S1P4 agonist (500 nM) \pm pertussis toxin (100 ng/ml). S1P4 agonist increases the transendothelial electrical resistance of PBMECs in the absence of pertussis toxin. Cotreatment of pertussis toxin and S1P4 agonist does, however, not ameliorate PT's barrier-opening effect, indicating G_i dependency of the tightening effect at the used concentration. The mean TEER value of three inserts per condition is shown. MBMECs, murine BMECs; ULOQ, upper level of quantification; LLOQ, lower level of quantification; PBMECs, porcine BMECs; PT, pertussis toxin; TEER, transendothelial electrical resistance.

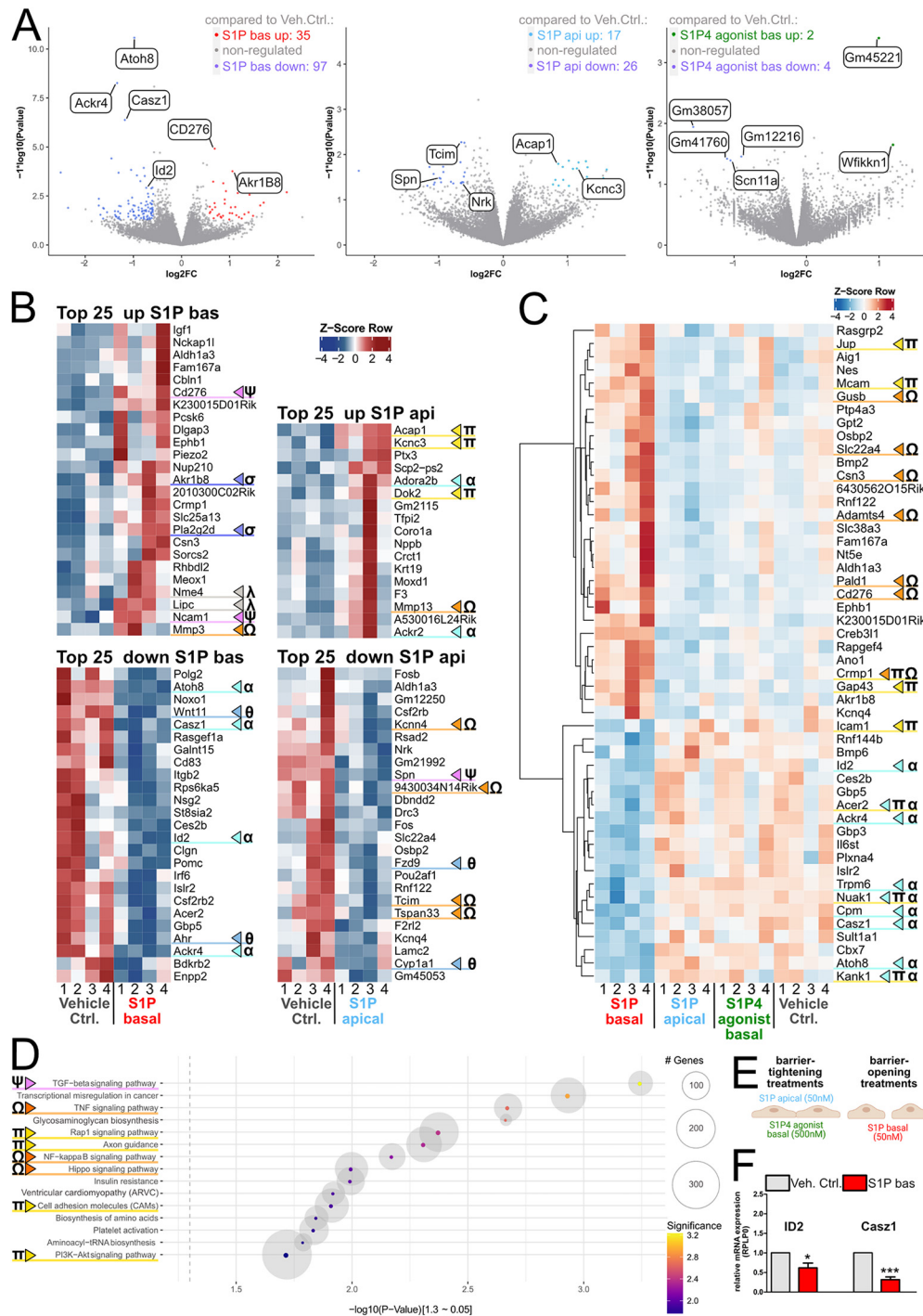


Figure 6. S1P receptor-binding pharmacological agents that either tighten or open endothelial barriers, respectively, induce functionally opposed transcriptional regulation patterns in MBMECs. RNA sequencing analysis of MBMECs was conducted 24 h after pharmacological treatment with functionally barrier-opening (50 nM S1P basal) or barrier-tightening (50 nM S1P apical or 500 nM S1P4 agonist basal) agents or the respective vehicle control. A summary of the different pharmacological treatment effects on MBMEC barriers is shown in panel E; $n = 4$ sets of MBMECs, 12 mice/n (both males and females). **A**, Volcano plots of regulated genes from the comparison between each of the three pharmacological treatments (S1P apical, S1P basal or S1P4 agonist basal) versus the respective vehicle control. Accepted transcripts: mean > 5 counts, $\log_2FC \pm 0.585$, $p \leq 0.05$. The number of significantly upregulated and downregulated genes for each of the treatments (compared with vehicle control) is indicated in each volcano plot's top corner. **B**, Z-score of the top 25 upregulated and top 25 downregulated genes on basal and apical S1P treatment, respectively. Accepted transcripts: mean > 5 counts, $\log_2FC \pm 0.585$, $p \leq 0.05$. Genes of particular relevance for endothelial barrier function and phenotype are highlighted with Greek letters and colored markings (homeostasis: cyan α , lipid metabolism: gray λ , dedifferentiation markers: purple ψ , oxygen stress response: dark blue σ , Wnt pathway regulation: light blue θ , inhibition of migration: yellow π , inflammation: orange Ω). **C**, Z-score of the top 50 regulated genes between apical versus basal S1P treatment. S1P4 agonist and vehicle control treatments are furthermore displayed for comparison. Accepted transcripts: mean > 5 counts, $\log_2FC \pm 0.585$, $p \leq 0.05$. Genes associated with endothelial barrier function and phenotype are highlighted with Greek letters and colored markings (cytoskeleton structure and focal adhesion: yellow π , proinflammatory and disease-associated genes: orange Ω , prohomeostatic genes: cyan α). **D**, Gene set enrichment (KEGG pathway) analysis from significantly regulated genes (mean > 5 counts, $\log_2FC \pm 0.585$, $p \leq 0.05$) of the comparison of apical versus basal S1P treatment. Corrected $p < 0.2$, top 15 sets are shown. Pathways involved in endothelial phenotype and barrier function are highlighted (dedifferentiation: purple ψ , inflammation: orange Ω , cytoskeleton and focal adhesion: yellow π). **E**, Summary graphic of the functional effects of the different pharmacological S1P receptor modulator treatments on MBMEC barrier permeability. **F**, Verification of the downregulation of the barrier-protective transcriptional regulators ID2 and Casz1 via qPCR in MBMECs 24 h posttreatment with 50 nM basal S1P ($n = 6$, 5 mice/n). The

down for up to 48 h posttransfection [$p = 0.022$ (36 h), $p = 0.0004$ (48 h), paired t tests each; Fig. 4G,H], which was accompanied by a significant transcriptional downregulation of VE-Cadherin, Claudin 5, and Occludin [$p = 0.023$ (VE-Cadherin), $p = 0.003$ (Cldn5), $p = 0.015$ (Ocl), paired t tests each; Fig. 4I]. Of note, these barrier-hampering effects could be observed although we only achieved a partial ($49.5 \pm 7.3\%$ std) knock-down of S1P4 in primary MBMECs ($p = 0.0008$, paired t test). This finding suggests that even a moderate decrease in S1P4 signaling might lead to drastic functional consequences for endothelial barrier integrity.

S1P4 agonist tightens endothelial barriers and ameliorates the opening effect of basal S1P

Following our hypothesis of a protective, barrier-maintaining effect of S1P4 signaling on BMEC barriers, we conducted functional TEER experiments with a pharmacological agonist of S1P4. Using S1P4 KO and WT MBMECs cultured on transwell inserts that were basally treated with S1P4 agonist (Fig. 5A), we confirmed both the agonist's receptor specificity for S1P4 (Fig. 5B,C) and the impermeability of the endothelial barrier for the agonist for at least 8 h posttreatment ($p < 0.0001$ for all time-points, paired t tests each; Fig. 5D). This is a time point when the agonist's tightening effect on WT MBMECs can already be observed (Fig. 5B). ANOVA analysis of S1P4 agonist-treated and vehicle-treated WT and S1P4 KO MBMECs indicates significant differences in mean TEER values between the four groups ($p = 0.0006$, $F = 14.36$, $R^2 = 0.8116$; Fig. 5C). S1P4-agonist treatment increased WT MBMEC TEER values in comparison to control treatment ($p = 0.0190$, paired t test), but did not affect S1P4 KO MBMEC TEER values, indicating a specificity of the compound for S1P4.

To assess whether the S1P4-associated tightening effect could also be observed in nonmurine BMECs and to validate its dependence on G_i signaling, we performed basal treatment of PBMECs with S1P4 agonist \pm either S1P or the G_i -inhibitor pertussis toxin. (Fig. 5E). Indeed, we observed a slight tightening effect in PBMECs 24 h after S1P4 agonist treatment in comparison to control medium [$p = 0.02$ (vehicle vs agonist treatment, 24 h, paired t test); Fig. 5F,G]. Importantly, the S1P4 agonist could ameliorate the long-term barrier-opening effect of basal S1P [$p = 0.0009$ (10 h, S1P vs S1P+S1P4 agonist), $p = 0.0014$ (24 h, S1P vs S1P4 agonist), paired t tests each; Fig. 5G]. In order to gain a better understanding of the barrier-tightening effect observed on basal S1P4 agonist treatment, we furthermore conducted a proof-of-principle control experiment ($n = 1$) with pertussis toxin to exclude a nonspecific tightening effect of the agonist not related to G_i signaling (Fig. 5I). The S1P4 agonist's barrier-tightening effect was fully abolished by pertussis toxin, hinting toward a G_i dependency of the functional tightening effect. In line with this finding, qPCR analysis revealed a significantly increased mRNA expression of Rac1 and VE-Cadherin 24 h after S1P4 agonist compared with vehicle control treatment [$p = 0.019$ (Rac1), $p = 0.03$ (VE-Cadherin), paired t tests each; Fig. 5H].

←

experimental setup is shown in Figure 2A. The normalized level of gene expression after Veh. Ctrl. treatment was set to 1, bar graphs represent mean mRNA expression \pm SEM. Statistical significance was assessed by paired two-tailed Student's t test; * indicates significantly altered gene expression levels compared with Veh. Ctrl. treatment, exact p values are specified in the text. MBMECs, murine BMECs; bas, basal; api, apical.

S1PR signaling changes the transcriptional regulation of MBMECs

To further elaborate the mechanisms underlying S1P receptor signaling-associated effects on primary brain microvascular endothelial barrier function, we treated MBMECs with either apical S1P, basal S1P or S1P4 agonist (a summary of the applied treatments and their effects on MBMEC permeability is shown in Fig. 6E) and studied the resulting gene expression patterns via RNA sequencing analysis (dataset available at GEO, GSE163561). Genes were considered as significantly regulated if a logarithmic fold change of at least ± 0.585 , a mean value higher than 5 and a p value lower than 0.05 were reached. Our analysis revealed that basal S1P evoked the greatest number of transcriptional changes in comparison to vehicle control treatment (97 differentially expressed genes (DEGs) down, 35 DEGs up; Fig. 6A). Apical S1P treatment caused a downregulation of 26 and an upregulation of 17 genes. Interestingly, pharmacological treatment with S1P4 agonist merely downregulated four genes (among them Scn11a/NaV1.9, a voltage-gated sodium channel whose activity is regulated by G-proteins; Vanoye et al., 2013) and upregulated two genes, one of them being the protease inhibitor Wfikkn1 (Trexler et al., 2001).

Apical and basal S1P treatments promote contrasting gene expression patterns

A detailed analysis of the Top 25 upregulated and downregulated DEGs on either apical or basal S1P treatment in comparison to the respective vehicle control treatments indicates opposing gene expression patterns that strongly reflect the contrary permeability effects of apical versus basal S1P treatment (Fig. 6B). Upon apical S1P treatment, a condition associated with high S1P1 and S1P4, but low S1P2 expression, we primarily observed an upregulation of genes involved in the inhibition of endothelial migration and the promotion of cortical actin stabilization, focal adhesion and barrier integrity. The most significantly upregulated genes were Acap1, a small GTPase involved in integrin $\beta - 1$ recycling (Li et al., 2005) and Kcnc3/Kv3.3, a voltage-gated potassium channel regulating the stabilization of cortical actin filaments (Zhang et al., 2016). Many of the genes which were downregulated on apical S1P treatment are associated with endothelial inflammation. Some representative examples are Tcim/TC1, a positive regulator of NF- κ B transcriptional activity (Kim et al., 2009) and Kcnn4/KCa3.1, a calmodulin-regulated potassium ion channel that promotes nitric oxide synthase activity and contributes to the development of neuroinflammation, atherosclerosis, and kidney fibrosis (Wulff and Castle, 2010).

Basal S1P, a treatment associated with a high S1P1 and S1P2, but a low S1P4 expression, on the other hand resulted in a massive downregulation of various genes associated with a homeostatic, fully differentiated and barrier-protective endothelial phenotype. Upon basal S1P treatment, we found the transcriptional regulators AtoH8/Hath6, Casz1, and ID2 to be downregulated, which control endothelial differentiation and tube formation (Fang et al., 2014), promote endothelial focal adhesion (Charpentier et al., 2013) and control VE-Cadherin expression (Su et al., 2009), respectively. Besides, we found markers of endothelial dedifferentiation to be upregulated on basal S1P treatment, particularly CD276 (Kraan et al., 2014) and Ncam-1 (Bussolati et al., 2006).

Apical S1P and basal S1P4 agonist promote a homeostatic endothelial phenotype

When we compared the Top50 DEGs between apical and basal S1P treatment and added S1P4 agonist-treated and vehicle

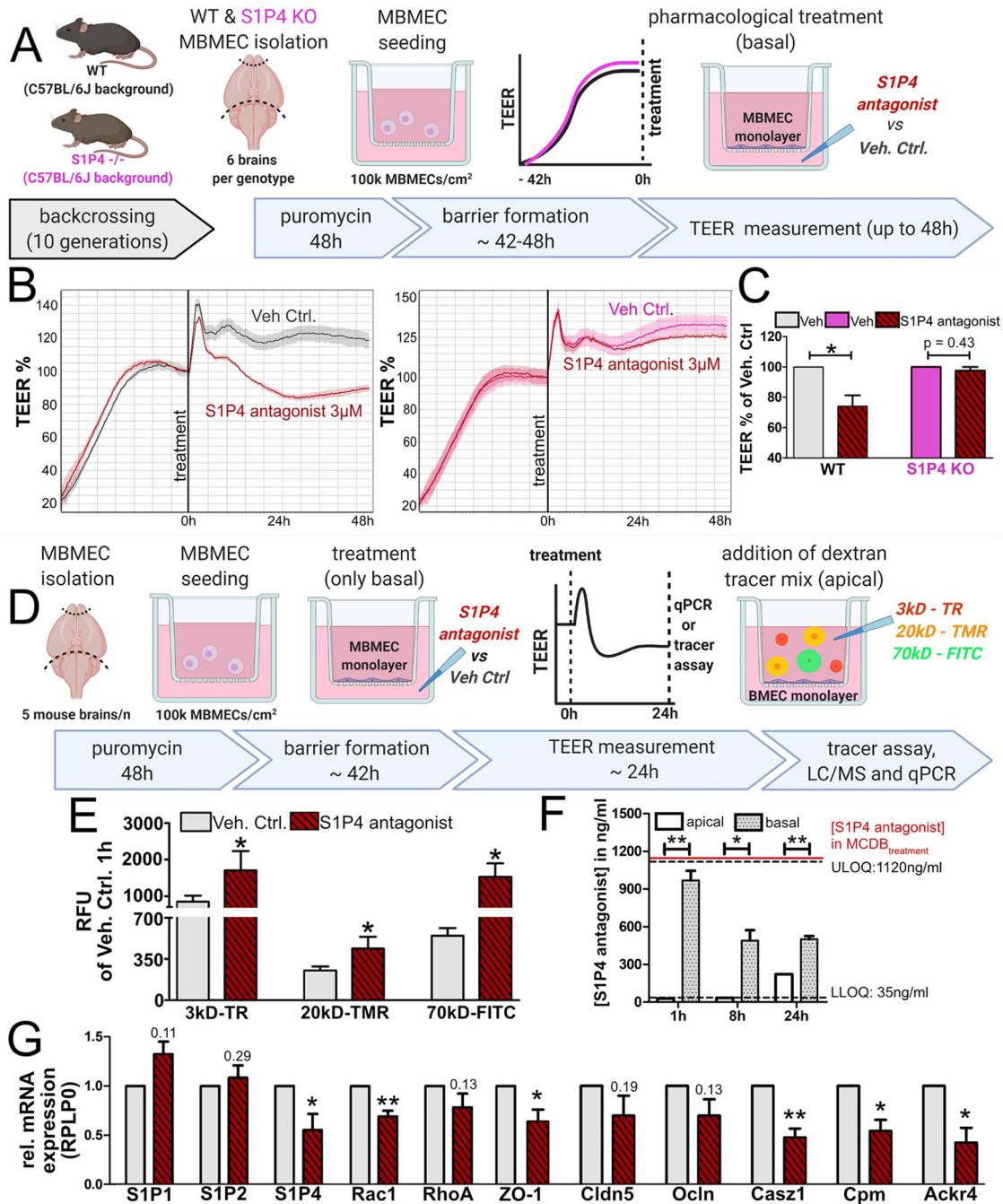


Figure 7. S1P4 antagonist opens MBMEC barriers *in vitro*. **A**, Methodology. After 10 generations of backcrossing S1P4 KO mice and C57BL/6J WT mice, brains from both male and female mice were used for MBMEC isolation ($n = 6$ sets of WT vs 3 sets of KO MBMECs, 6 mice/ n) to verify S1P4 antagonist specificity *in vitro*. **B**, Representative TEER graphs of the functional effect of the S1P4 antagonist CYM50358 on WT and S1P4 KO MBMECs. S1P4 antagonist ($3 \mu\text{M}$, basal treatment in a transwell setup) has an opening effect on WT but not S1P4 KO MBMEC barriers. The mean TEER value of three inserts per treatment group is shown. **C**, Statistical analysis of TEER values from the above experiment 24 h after S1P4 antagonist stimulation ($n = 6$ sets of WT vs 3 sets of S1P4 KO MBMECs, 6 mice/ n). TEER values of three inserts/condition/ n were used for analysis. TEER values after Veh. Ctrl. treatment were set to 100% for each genotype. Bar graphs represent mean TEER values \pm SEM. Statistical significance of mean differences between the four groups was confirmed via ANOVA ($p = 0.003$, $F = 7.584$, $R^2 = 0.62$). Statistical significance between two treatment groups of the same genotype was assessed via paired two-tailed Student's t test; * indicates significantly different mean TEER values between the compared treatment groups, exact p values are specified in the text. **D**, Methodology. MBMECs were treated with S1P4 antagonist ($3 \mu\text{M}$) or vehicle control medium from the basolateral side in a transwell setup ($n = 16$ sets of MBMECs, 5 mice/ n , both sexes). From four sets of MBMECs, apical and basolateral supernatant was harvested at 1 h, 8 h and 24 h posttreatment to assess barrier permeability of the compound. 24 h posttreatment, six sets of MBMECs were harvested for qPCR analysis, the remaining six sets were used for permeability assessment with different-size dextran tracers. **E**, Relative fluorescence intensity (RFU) of different-size dextran tracers (TR, 3 kDa; TMR, 20 kDa; and FITC, 70 kDa) in basal supernatant of S1P4 antagonist-treated or vehicle-treated MBMECs from the above experiment 4 h after tracer addition; $n = 6$ (5 mice/ n , 6 inserts/condition/ n were analyzed). A scale break was inserted into the y -axis to more clearly resolve the RFU values of the different-size dextran tracers that were used. Statistical significance between antagonist treatment and vehicle control group was assessed via paired two-tailed Student's t test; * indicates significant RFU differences compared with Veh. Ctrl. treatment, exact p values are specified in the text. **F**, LC/MS analysis of S1P4 antagonist concentrations detected in apical and basal supernatant of WT MBMECs ($n = 4$ sets of supernatant per compartment and time, 5 mice/ n , both sexes) in a transwell setup at 1, 8, and 24 h after basal stimulation with $3 \mu\text{M}$ S1P4 antagonist. Bar graphs represent mean S1P4 agonist concentrations \pm SEM. For at least 8 h poststimulation, S1P4 antagonist was undetectable in apical supernatant, indicating barrier impermeability for the compound at early timepoints. Statistical significance between apical and basal S1P concentrations was assessed for each time point by paired two-tailed Student's t test. **G**, Relative mRNA expression (normalized to RPLP0) of the endothelial S1P receptors, Rac1, RhoA, tight junction molecules, and the barrier-protective genes Casz1, Cpm, and Ackr4 in MBMECs from the above

control groups for comparison (Fig. 6C), a distinct pattern of transcriptional regulation became apparent. We found homeostasis-associated and differentiation-promoting endothelial transcriptional regulators like *AtoH8*, *ID2*, and *Cas1* to be constitutively expressed in all treatment groups with the exception of basal S1P. Besides, multiple genes which have previously been suggested to perform an anti-inflammatory or barrier-protective function like *Cpm* (Sørensen-Zender et al., 2019), *Ackr4* (Nibbs and Graham, 2013), and *Trpm6* (Ghabriel and Vink, 2011) were steadily expressed in all treatment groups and solely downregulated on basal S1P. Fittingly, genes associated with endothelial migration and/or inflammation like *CD276* (Kraan et al., 2014), *Mcam/CD146* (Kang et al., 2006), and *Adams4* (Wågsäter et al., 2008), were solely upregulated on basal S1P with a much lower expression in the other treatment groups. Our data thus indicate that both barrier-tightening treatments were associated with a homeostatic gene expression pattern and the promotion of full endothelial differentiation.

Importantly, we found *Kank1* and *Crmp1*, two genes that critically affect cytoskeleton structure by altering the balance between barrier-protective Rac and barrier-disruptive Rho signaling in opposite directions (Kakinuma et al., 2008; Mukherjee et al., 2009), to be among the Top50 DEGs between apical and basal S1P treatment (Fig. 6C). While basal S1P treatment was associated with a downregulation of *Kank1* and upregulation of *Crmp1* (a combination that favors barrier-disruptive Rho signaling), all treatments associated with functional barrier integrity (including vehicle control treatment) instead promoted the very opposite *Kank1* and *Crmp1* expression pattern which favors Rac1 predominance and barrier integrity.

Basal S1P promotes endothelial dedifferentiation and inflammation and disturbs homeostasis

KEGG pathway analysis of DEGs between apical and basal S1P treatment indicates their involvement in TGF- β signaling, Rap1 signaling, NF- κ B signaling and multiple other pathways regulating endothelial differentiation, migration and inflammation (Fig. 6D). As we were particularly interested in the mechanisms underlying the barrier-opening effect of basal S1P, we re-analyzed qPCR samples from our previous TEER experiments (Fig. 2B,G) for a putative loss of the barrier-protective transcriptional regulators *ID2* and *Cas1* and could indeed confirm the downregulation of these genes on basal S1P treatment (*ID2*: $p = 0.026$, $t = 3.124$, $df = 5$, paired t test; *Cas1*: $p = 0.0002$, $t = 9.946$, $df = 5$, paired t test; Fig. 6F).

S1P4 antagonist opens BMEC barriers *in vitro* and *in vivo*

With a better understanding of the transcriptional regulation patterns associated with decreased S1P2 expression (apical S1P treatment) versus decreased S1P4 expression (basal S1P treatment) in MBMECs, we continued to analyze the effect of S1P4 signaling inhibition. We used a pharmacological S1P4 antagonist to validate that it was indeed the lack of S1P4 signaling (and not merely S1P2 activation) which induced the observed barrier-opening effects on basal S1P. As expected, TEER measurements

indicate a strong long-term barrier-opening effect on basal S1P4 antagonist treatment of WT MBMECs, but not S1P4 KO MBMECs (Fig. 7A,B). Statistical analysis indicates significantly different mean TEER values between vehicle and S1P4 antagonist-treated WT and KO MBMECs ($p = 0.0030$, $F = 7584$, $R^2 = 0.6191$, ANOVA; Fig. 7C) with S1P4 antagonist significantly decreasing the resistance of WT ($p = 0.016$, paired t test), but not S1P4 KO endothelial monolayers ($p = 0.43$, paired t test), indicating the compound's specificity for S1P4. LC/MS analysis furthermore confirmed the impermeability of the endothelial barrier for basal S1P4 antagonist for at least 8 h posttreatment [$p = 0.001$ (1 h), $p = 0.012$ (8 h), $p = 0.002$ (24 h), paired t tests each; Fig. 7F], a time point when the antagonist's opening effect on WT MBMECs can already be observed (Fig. 7B). Apart from its effect on TEER values, basal S1P4 antagonist treatment also increased the permeability of WT MBMEC barriers for different-size dextran tracer molecules (Fig. 7E). In comparison to vehicle control treatment, we found S1P4 antagonist to increase the extravasation of tracers ranging in size from 3 to 70 kDa [$p = 0.047$ (3-kDa-TR), $p = 0.039$ (20-kDa-TMR), $p = 0.017$ (70-kDa-FITC), paired t tests each]. In accordance with these findings, qPCR analysis (Fig. 7G) revealed a significant downregulation of *Rac1* ($p = 0.003$), *Tjp/ZO-1* ($p = 0.029$) and the barrier-protective RNA sequencing DEGs *Cas1* ($p = 0.002$), *Cpm* ($p = 0.01$) and *Ackr4* ($p = 0.02$, paired t tests each) in S1P4 antagonist-treated MBMECs. Besides, we found no regulation of S1P1 or S1P2 expression, but observed a significant downregulation of S1P4 on antagonist treatment ($p = 0.041$, paired t test), pointing toward the involvement of S1P4 signaling for the maintenance of the above-mentioned barrier-protective factors' expression. The *in vitro* barrier opening effect of S1P4 antagonist on WT MBMECs was also observed *in vivo* after S1P4 antagonist pretreatment of WT and S1P4 KO mice (Fig. 8A), the extravasation of fluorescent 20-kDa dextran tracer into the brain parenchyma of WT, but not S1P4 KO, mice was significantly higher in the S1P4 antagonist-treated group compared with the control vehicle group (Fig. 8B). Statistical analysis indicates significantly different tracer extravasation levels between vehicle and S1P4 antagonist-treated WT and S1P4 KO mice ($p < 0.0001$, $F = 12.66$, $R^2 = 0.452$, ANOVA) with S1P4 antagonist significantly increasing WT BBB permeability ($p = 0.0004$, paired t test), but not affecting S1P4 KO BBB permeability ($p = 0.64$, paired t test). These data indicate a S1P4-specific opening effect of the antagonist not only *in vitro*, but also *in vivo*. For less tight endothelial barriers of lung and kidney we observed no change in endothelial permeability for tracer molecules on S1P4 antagonist treatment. Interestingly, our experiment furthermore indicated a strong tendency for decreased tracer extravasation into the brain parenchyma of vehicle-treated S1P4 KO in comparison to WT mice ($p = 0.053$, $t = 2.038$, $df = 23$, unpaired t test).

S1P4 KO MBMECs show decreased S1P2 expression levels

To better understand the unexpected BBB phenotype of S1P4 KO mice (which was in tendency tighter than WT; Fig. 8B), we assessed S1PR expression levels in WT and S1P4 KO MBMECs via qPCR analysis and investigated the transcriptional differences in MBMECs from both genotypes via RNA sequencing (sequencing dataset available at GEO, GSE163561; Fig. 9). Interestingly, qPCR analysis indicated a significant downregulation of S1P2 in S1P4 KO MBMECs with mean S1P2 expression level in KO cells reaching only 48% of WT expression levels ($p = 0.0014$, unpaired t test; Fig. 9B). Of note,

←

experiment 24 h posttreatment ($n = 6$, 5 mice/n). The normalized level of gene expression after Veh. Ctrl. treatment was set to 1. Bar graphs represent mean mRNA expression \pm SEM. Statistical significance was assessed by paired two-tailed Student's t test; * indicates significantly altered gene expression levels compared with Veh. Ctrl. treatment, exact p values are specified in the text.

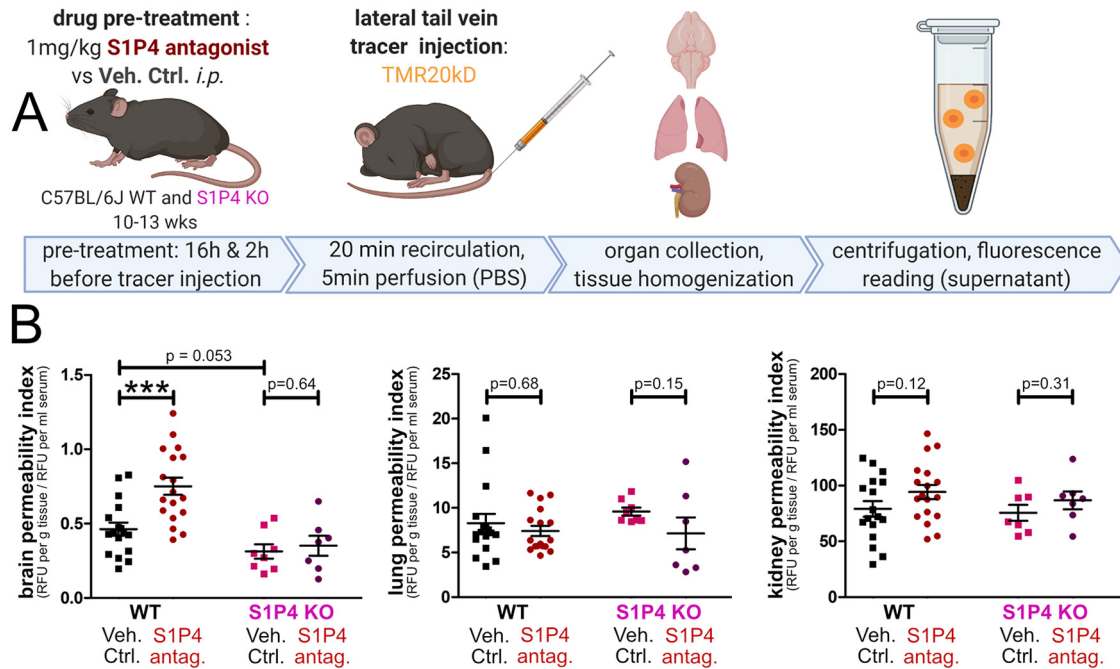


Figure 8. S1P4 antagonist opens the blood-brain barrier of mice *in vivo*. **A**, Methodology of the S1P4 antagonist treatment of WT (C57BL/6J) and S1P4 KO mice. Mice were pretreated with S1P4 antagonist (1 mg/kg, injected 16 and 2 h before permeability assessment) or vehicle control, respectively. TMR 20-kDa dextran tracer was injected into the lateral tail vein. After 20-min tracer circulation and 5-min perfusion, brain, kidney and lung were harvested, homogenized, and supernatant fluorescence was measured to assess endothelial permeability in the different organs. **B**, Permeability index (RFU normalized to serum levels and tissue weight) of brain, lung and kidney homogenate from S1P4 antagonist-treated or vehicle-treated WT and S1P4 KO mice from the above experiment; $n = 18$ S1P4 antagonist-treated WT mice versus 17 vehicle-treated WT mice (male and female, 10–13 weeks old). S1P4 KO mice ($n = 7$ S1P4 antagonist-treated KO mice vs 8 vehicle-treated KO mice, male and female, 10 weeks old) were used to validate S1P4 antagonist specificity *in vivo*. Data are represented as vertical scatter plot, mean permeability index values of each treatment group \pm SEM are shown. D'Agostino and Pearson omnibus normality test was used to assess normal distribution of data ($\alpha \leq 0.05$ for WT lung permeability indices, for all other permeability indices $\alpha > 0.05$). Statistical significance between S1P4 antagonist and vehicle control treatment groups was assessed by unpaired two-tailed Student's *t* test for brain and kidney permeability indices and by Mann–Whitney test for lung permeability indices. Statistical significance between WT and S1P4 KO brain permeability indices was assessed by unpaired two-tailed Student's *t* test; * indicates a significantly different mean permeability index compared with the vehicle control treatment group, exact *p* values are specified in the text. *i.p.*, intraperitoneal; RFU, relative fluorescence unit.

S1P1 expression was not significantly altered in S1P4 KO MBMECs ($p = 0.70$, unpaired *t* test) and S1P4 was undetectable, therein confirming homozygous S1P4 ablation. PANTHER pathways analysis of DEGs between WT and S1P4 KO MBMECs confirmed that S1P2 downregulation in S1P4 KO MBMECs was associated with significantly altered expression levels of many genes that are involved in S1P2-associated and/or RhoA-associated intracellular signaling pathways (Fig. 9D). This finding plausibly explains the unexpectedly tight BBB phenotype of S1P4 KO mice, although the detailed mechanisms which cause the S1P2 downregulation remain elusive. A thorough analysis of the most significantly altered DEGs between WT and S1P4 KO MBMECs, however, indicated a bidirectional and seemingly random upregulation and downregulation of both barrier-protective and barrier-disruptive genes in S1P4 KO MBMECs (Fig. 9B). Importantly, many of the DEGs that were involved in these complex transcriptional regulation patterns between S1P4 KO and WT MBMECs were either associated with endothelial barrier disruption, dedifferentiation or inflammation. Although the precise details how S1P2 and S1P4 interact with each other on a transcriptional and protein level in BMECs remain unclear, our findings clearly indicate that the interplay of these two S1PRs may be of significant relevance for the regulation of BBB integrity and homeostasis.

Discussion

In the past years, much information has been gathered about the role of endothelial S1P1 and S1P2 signaling for the regulation of

BBB permeability. However, the extent of S1P's influence on brain endothelial permeability is not entirely understood yet, and particularly the role of other endothelial S1P receptors remains largely unknown. In the current study, we report an apical tightening and basal opening effect of S1P in primary BMECs and therefore hypothesized that S1P-mediated permeability is regulated by polarized S1P receptors distribution at the BBB. We demonstrate a critical role of endothelial S1P4 receptor for BBB permeability regulation and show its abluminal localization on BMECs, in line with a recent report on S1P1's abluminal membrane localization (Nitzsche et al., 2021).

Apical S1P functionally tightens BMEC barriers and promotes a homeostatic phenotype

Under physiological conditions, luminal S1P concentrations in blood plasma at the apical side of BMECs greatly exceed S1P concentrations in brain parenchyma at the abluminal side. Indeed, we found apical S1P treatment in our transwell TEER setup to promote endothelial barrier integrity both in MBMEC and PBMECs (Fig. 2B,D, C,E, respectively). Importantly, qPCR analysis indicates that the only S1P receptor whose transcription is significantly altered on apical S1P treatment, is S1P2 (mean expression decrease by $68.2 \pm 24.6\%$ std; Fig. 2G). S1P2 is known to induce NF- κ B activation via $G_{12/13}$ (Zhang et al., 2013), which, in turn, has been reported to stabilize the transcription factor *Snail* (Wu et al., 2009), a known inducer of endothelial-to-mesenchymal transition (EndMT) and junctional molecule degradation (Stenmark et al., 2016). Fittingly, our RNA sequencing

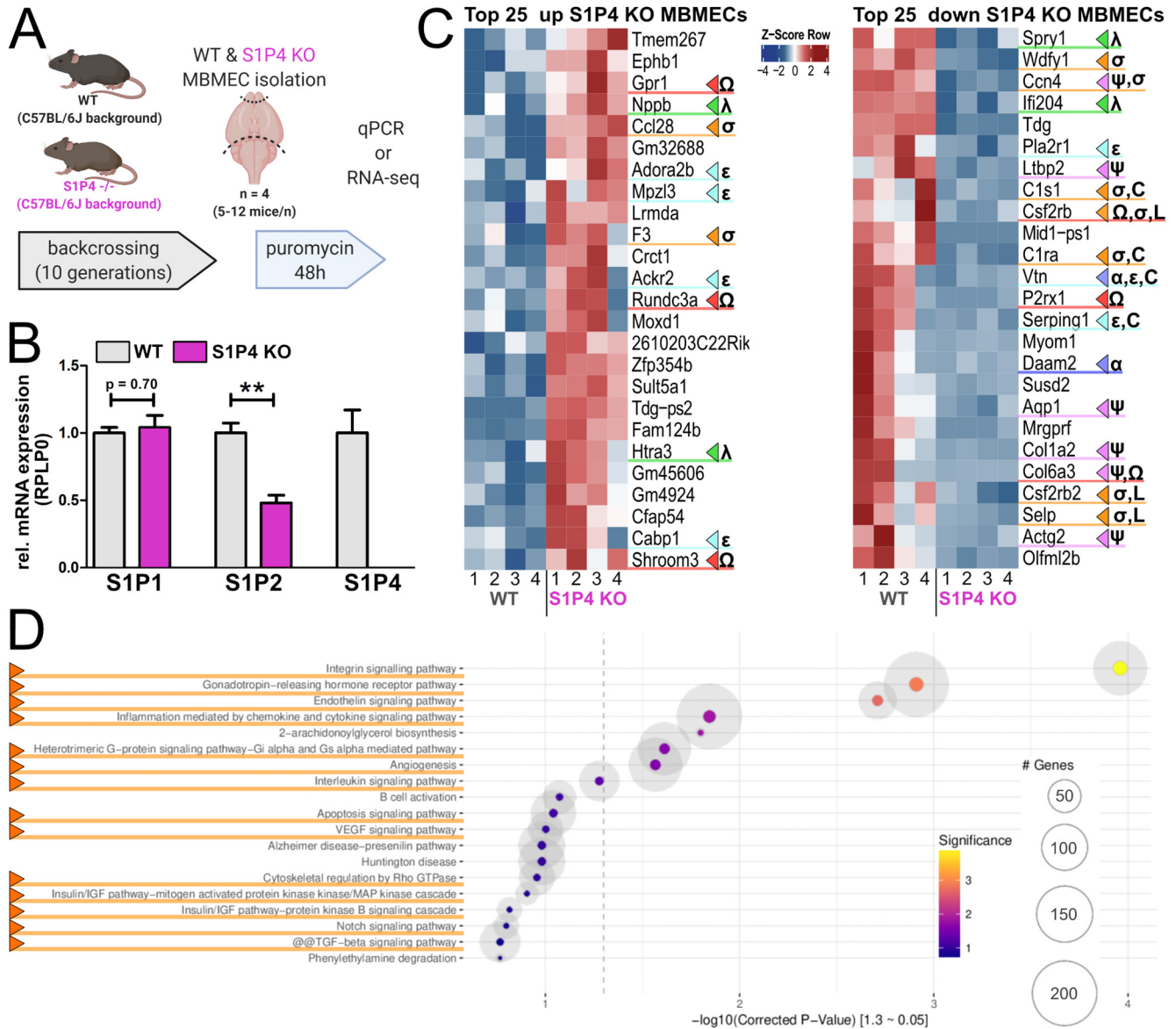


Figure 9. S1P2 transcription is downregulated in S1P4 KO MBMECs. **A**, Methodology. Brains from both male and female S1P4 KO and C57BL/6J WT mice were used for MBMEC isolation. Cells were harvested for mRNA analysis via qPCR and RNA sequencing immediately after 48 h puromycin treatment. **B**, Relative mRNA expression levels (normalized to RPLP0) of endothelial S1PRs in WT and S1P4 KO MBMECs after 48 h puromycin treatment ($n = 4$ sets of MBMECs per genotype, 5 mice/n). The relative average S1PR gene expression level in WT mice was set to 1. Bar graphs represent mean mRNA expression \pm SEM. Statistical significance was assessed by unpaired two-tailed Student's t test. As expected, S1P4 KO MBMECs did not express S1P4. **C**, Z-score of the top 25 upregulated and top 25 downregulated genes between WT and S1P4 KO MBMECs. Accepted transcripts: mean > 5 counts, $\log_2fc \pm 0.585$, $p \leq 0.05$. Genes of particular relevance for endothelial barrier function and phenotype are highlighted with Greek and Roman letters and colored markings (barrier protection: dark blue α , barrier disruption: red Ω , inhibition of inflammation: cyan ε , promotion of inflammation: orange σ , dedifferentiation: purple ψ , inhibition of dedifferentiation: green λ , complement cascade activation: C, leukocyte adhesion: L). **D**, Gene set enrichment (PANTHER pathway) analysis from significantly regulated genes (mean > 5 counts, $\log_2fc \pm 0.585$, $p \leq 0.05$) between WT and S1P4 KO MBMECs ($n = 4$, 12 mice/n). Corrected $p < 0.2$, the top 20 sets are shown. Pathways that are controlled by S1P2 signaling (or RhoA/ROCK activity) are highlighted with an orange marker. MBMECs, murine MBMECs.

data reveals that apical S1P increases the expression of genes which inhibit NF- κ B activation, whereas genes that promote NF- κ B activation and dedifferentiation are downregulated (Fig. 6B). The low S1P2 transcription rate we observed after apical S1P treatment matches previous findings of a hardly detectable S1P2 protein expression in homeostatic brain MVs *in vivo* (Kim et al., 2015). Overall, we found apical S1P treatment to promote endothelial barrier integrity and a homeostatic, fully differentiated endothelial phenotype characterized by low S1P2 and high S1P1 and S1P4 expression. Our TEER and RNA sequencing data thus confirm previous findings about the barrier-protective effects of apical S1P treatment (Garcia et al., 2001; Singleton et al., 2005).

Basal S1P opens BMEC barriers and promotes endothelial dedifferentiation

TEER measurements and dextran tracer permeability assays indicate a long-term permeability increase in MBMECs and PBMECs after basal S1P treatment (Figs. 2B–F, 7F,G). As expected, qPCR and WB analyses indicate decreased junctional molecule expression levels after basal S1P treatment of MBMECs (Figs. 2G, 3B,D). Surprisingly, however, the only S1P receptor whose expression we found altered by basal S1P treatment was not the barrier-disruptive S1P2, but instead S1P4, a receptor hitherto unknown for its effects on endothelial permeability. RNA sequencing indicates that multiple prohomeostatic endothelial transcriptional regulators

that influence junction molecule expression, focal adhesion and endothelial differentiation are massively downregulated on basal S1P treatment, whereas genes associated with endothelial inflammation and dedifferentiation are upregulated (Fig. 6B, C). In the context of BBB breakdown after ischemic stroke, a condition associated with high S1P concentrations in brain parenchyma (Salas-Perdomo et al., 2019), endothelial polarity loss and TGF- β -dependent EndMT have very recently been reported (Chen et al., 2020; Ma et al., 2020). Along these lines, S1P-induced cross-activation on Smad signaling has been reported to mimic the effects of TGF- β signaling in mesangial cells (Xin et al., 2004). Interestingly, dihydro-S1P, a receptor modulator that preferentially binds and activates S1P4 (Inagaki et al., 2005), has been shown to inhibit said cross-activation (Bu et al., 2008), possibly pointing toward S1P4's ability to prevent S1P-induced TGF- β signaling. Park and Im (2019) have recently demonstrated that S1P2 signaling promotes TGF- β -associated epithelial-to-mesenchymal transition in the lung and S1P4's ability to prevent S1P2 internalization and signaling induction has been shown in breast cancer cells (Ohotski et al., 2014). We therefore hypothesize that S1P4 is involved in the regulation of S1P2-dependent TGF- β signaling and EndMT in BMECs. This hypothesis fits our KEGG pathway analysis of DEGs between apical and basal S1P treatment (Fig. 6D) and the downregulation of both S1P2 and dedifferentiation-associated genes in S1P4 KO MBMECs (Fig. 9B,C). In summary, we found basal S1P treatment to promote massive endothelial barrier disruption and a partly dedifferentiated endothelial phenotype characterized by high S1P1 and S1P2, but low S1P4 expression.

S1PR expression levels in BMECs regulate the balance between G_i and G_{12/13} signaling, therein determining endothelial phenotype and barrier tightness

Many of the barrier-disruptive transcriptional changes we observed on basal S1P treatment (Fig. 6B,C), have previously been reported as a result of either S1P2 (and thus G_{12/13}) signaling or a disruption of S1P1 (and thus G_i) signaling (Takuwa et al., 2013; Zhang et al., 2013; Perry et al., 2016). A growing body of evidence indicates that the relative balance between G_i and G_{12/13} activity determines the overall functional outcome and endothelial phenotype caused by S1P (Reinhard et al., 2017). We found apical S1P to promote a massive transcriptional downregulation of S1P2 (which apparently results in a decreased G_{12/13} activity as indicated by the RNA sequencing DEGs). In a very similar, albeit functionally antithetical fashion, basolateral S1P promoted a strong downregulation of S1P4 (which apparently resulted in decreased G_i activity as indicated by the observed RNA sequencing DEGs). This hypothesis is also supported by qPCR analysis after S1P4 antagonist treatment indicating a decreased Rac1 expression (Fig. 7G). Singleton et al. (2005) have

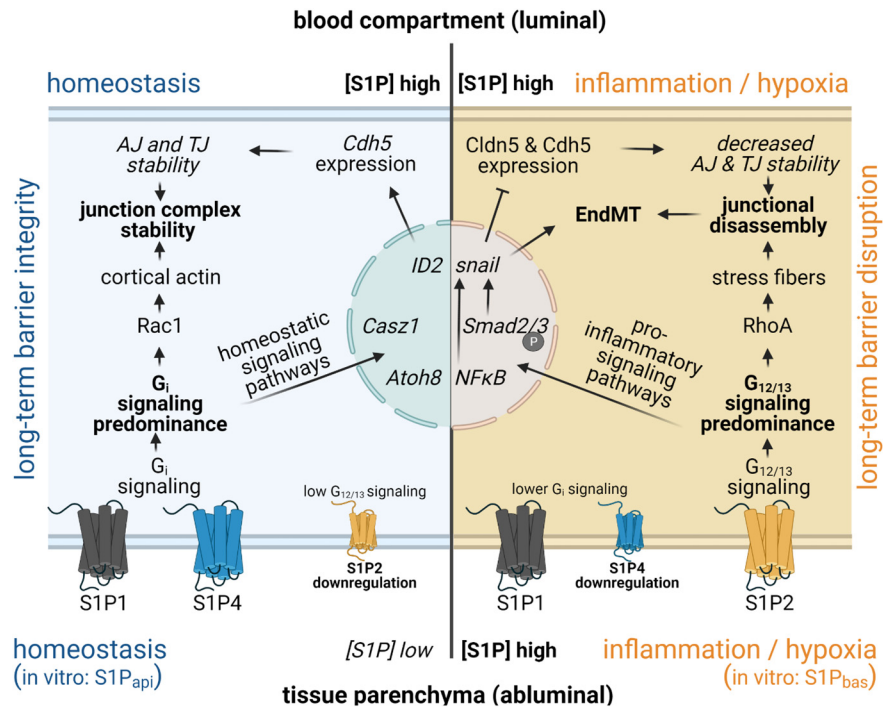


Figure 10. Endothelial S1P receptor signaling at the blood-brain barrier in health and disease. Under homeostatic conditions, S1P concentrations are high on the luminal and low on the abluminal side of brain microvascular ECs. Owing to BBB tightness, only few S1P molecules reach the abluminal endothelial membranes (either via transcytosis of plasma S1P or the export of intracellular endothelial S1P by transport proteins) where they primarily activate S1P1 and S1P4, the two most abundantly expressed endothelial S1P receptors in homeostasis. The high expression of endothelial S1P1 and S1P4 and low expression of S1P2 promotes G_i signaling, Rac1 activity and the expression of prohomeostatic endothelial transcription factors like ID2, Atoh8, and Casz1. In consequence, high junctional molecule (particularly Cdh5 an adherens junction (AJ) molecule and Cldns a tight junctions (TJ) molecule and Cldn5) expression levels enhance interendothelial junctional stability and promote long-term barrier integrity. Under pathologic conditions (like hypoxia or inflammation), however, leakage of plasma S1P into the brain tissue parenchyma and/or local S1P release from endothelial cells or resident brain cells (such as astrocytes or pericytes) may occur on the abluminal side of brain microvascular ECs. Our data indicate high abluminal S1P concentrations to cause a relative downregulation of endothelial S1P4 (and thus presumably a decrease in barrier-protective G_i signaling) and a relative upregulation of endothelial S1P2 (and thus presumably an increase in barrier-disruptive G_{12/13} signaling). Decreased endothelial S1P4 receptor expression is therefore associated with a shift from prohomeostatic toward proinflammatory G-protein signaling pathways that are associated with enhanced RhoA activity and increased NfκB and TGF- β signaling. Eventually, this may result in decreased junctional molecule expression, the disassembly of interendothelial junctional complexes, the onset of EndMT and a long-term impairment of the blood-brain barrier.

reported similar observations regarding S1P1 inhibition which resulted in (G_i-dependent) reduction of Rac1 activity, the disassembly of cortical actin and increased permeability in lung endothelial cells. Along these lines, FTY720, an FDA-approved functional antagonist of S1P1, S1P3, S1P4 and S1P5 for the treatment of MS is known to cause receptor internalization and degradation (Matloubian et al., 2004). As G_i/Rac1 and G_{12/13}/RhoA reciprocally inhibit each other's activity (Reinhard et al., 2017), we hypothesize S1P4-associated G_i signaling to inhibit barrier-disruptive RhoA activity in BMECs. In support of this hypothesis, Feng et al. (2018) have demonstrated that RhoA activity decreases ZO-1 expression in BMECs which matches our observation of decreased ZO-1 transcription levels after S1P4 antagonist treatment (Fig. 7G) and basal S1P treatment (Fig. 2G). It is thus very tempting to speculate that S1P4's barrier-enhancing effects might be explained by its contributions to G_i-mediated Rac1 activation and tight junctional stabilization. In line with this hypothesis, our TEER data confirms that the barrier-tightening effect of S1P4 agonist on BMECs is fully abolished by pertussis toxin (Fig. 5I). Vehicle control treatment (a condition associated with relatively high S1P4, but also relatively high S1P2 expression levels; Fig. 2G) is nevertheless associated with barrier integrity (Fig. 2B,D) and prohomeostatic gene expression (Fig.

6C). This indicates that endothelial permeability is not merely induced by S1P2 upregulation, but rather depends on the relative balance between barrier-protective (S1P1 and S1P4-mediated) and barrier-disruptive (S1P2-mediated) G-protein signaling pathways (as proposed by Reinhard et al., 2017). Importantly, the tight BBB phenotype of S1P4 KO mice (Fig. 8B) indicates that although a great amount of evidence points toward S1P4's crucial relevance for the maintenance of G_i signaling predominance in homeostatic WT MBMECs (Figs. 2G, 5H, 6C, 7G), its constitutive genetic ablation can apparently be fully compensated in KO animals. The molecular mechanisms which regulate endothelial S1PR expression levels in BMECs (particularly in S1P4 KO mice) remain elusive, however, we hypothesize that the complex bidirectional regulation patterns of barrier permeability-associated genes that we observed in S1P4 KO MBMECs (Fig. 9C) are associated with compensatory gene regulation because of S1P4 deletion and S1P2 downregulation. As the BBB of both WT and S1P4 KO mice is tight in physiological conditions, our observations of lower tracer permeability in S1P4 KO compared with WT animals (Fig. 8B) also suggest a potential impact of S1P4 signaling on circumventricular organs that do not possess a tight barrier (Benz et al., 2019). Further research on S1P2's and S1P4's putative influence on each other's transcription levels and signaling activity (Ohotski et al., 2014) is clearly required to fully understand the effects of endothelial S1PR signaling at the BBB. In summary, we suggest S1P4 to be a novel player alongside of S1P1 and S1P2 that contributes to BBB permeability regulation by influencing the relative balance between G_i and G_{12/13} activity in BMECs. We propose that S1P4 signaling significantly contributes to endothelial barrier integrity and differentiation.

Endothelial S1P4 is a novel regulator of brain microvascular permeability

Our data strongly indicate that S1P4 promotes MBMEC and PBMEC barrier integrity in different model systems *in vitro* and *in vivo*. In stroke, a neurologic disease associated with BBB dysfunction, our data from ischemic and contralateral murine brain hemispheres indicate a downregulation of S1P4 in the infarct hemisphere both on mRNA and protein level (Fig. 4B–E). Taken together with our *in vitro* data of S1P4 downregulation after basal S1P treatment (Figs. 2G, 3C,D), these findings indicate a correlation between BMEC barrier impairment and decreased S1P4 expression. Causal barrier-protective effects of S1P4 signaling are furthermore directly indicated by the barrier-tightening effect of the pharmacological S1P4 agonist observed in functional TEER experiments (Fig. 5C,G). Besides, causality of S1P4 inhibition-associated barrier breakdown induction is indicated by long-term barrier impairment in TEER and tracer permeability experiments on S1P4 knock-down and after antagonist treatment in BMECs *in vitro* (Figs. 4G,H, 7C,E) and the increased BBB permeability for tracer molecules after S1P4 antagonist treatment of WT mice *in vivo* (Fig. 8B). The respective functional effects after basal S1P4 agonist and antagonist treatment of BMECs already occur at timepoints when compounds are undetectable in apical supernatants (Figs. 5D, 7F), a finding which supports our hypothesis of S1P4's primarily abluminal localization (Fig. 3F) on a functional level. Most importantly, even a partial knock-down of S1P4 ($49.5 \pm 7.3\%$ std) in MBMECs was already sufficient to decrease the expression of VE-Cadherin, Occludin, and Claudin 5, the three most important determinants of interendothelial barrier integrity (Fig. 4I). One important question that remains unanswered by our data are the mechanism underlying the S1P4 agonist-mediated rescue of endothelial

barrier breakdown after basal S1P treatment of PBMECs (Fig. 5F,G). We hypothesize that the lack of transcriptional differences between basal S1P and rescue treatment after 24 h (Fig. 5H) is associated with the reversibility of the barrier opening effect in PBMECs (which spontaneously start to recover from barrier breakdown about 24 h after basal S1P treatment; Fig. 5F). Further research is needed to clarify the mechanisms facilitating the reversibility of barrier opening in PBMECs to explain the observed interspecies differences and assess the situation in human BMECs.

In summary, our data strongly indicate a barrier-protective role of the endothelial S1P4 receptor for primary BMECs *in vitro* and *in vivo*. We found decreased S1P4 expression and signaling (on S1P4 siRNA, basal S1P, and S1P4 antagonist treatment, respectively) to be associated with a functional endothelial barrier breakdown and a decreased expression of essential prohomeostatic endothelial transcriptional regulators and junctional molecules. Conversely, S1P4 agonist tightened BMEC barriers and rescued the barrier-disruptive effect of basal S1P. Overall, our data suggest that in a homeostatic physiological situation with high luminal and low abluminal S1P concentrations, robust S1P4 expression and signaling promote G_i-mediated endothelial homeostasis and barrier protection that favors the transcriptional downregulation of S1P2 and decreases G_{12/13} signaling (Fig. 10). In pathologic situations with high abluminal S1P concentrations, however, we found indication of a transcriptional downregulation of S1P4 that appears to promote a switch from barrier-protective S1P1 and S1P4-mediated G_i signaling toward S1P2-mediated, barrier-disruptive G_{12/13} signaling. From this point of view, the abluminal localization of S1P4 on BMECs might serve as a crucial sensor for the detection of unphysiologically high S1P concentrations within the brain parenchyma and the initiation of a proper endothelial response that enables immune cell infiltration, promotes tissue repair and eventually supports neuroprotection and neovascularization. Further research is needed to clarify the precise localization and possible interactions of all endothelial S1P receptors. Pharmacological drug development might greatly benefit from a deeper knowledge of S1P receptor signaling and the resultant effects on different cell types at the NVU. In this regard, we particularly suggest further research on the therapeutic potential of S1P4 agonists for the treatment of acute and chronic neurologic diseases characterized by neurovascular impairment.

References

- Aoki M, Aoki H, Ramanathan R, Hait NC, Takabe K (2016) Sphingosine-1-phosphate signaling in immune cells and inflammation: roles and therapeutic potential. *Mediators Inflamm* 2016:8606878.
- Benz F, Wichitnaowarat V, Lehmann M, Germano RF, Mihova D, Macas J, Adams RH, Taketo MM, Plate KH, Guérit S, Vanhollenbeke B, Liebner S (2019) Low wnt/ β -catenin signaling determines leaky vessels in the subfornical organ and affects water homeostasis in mice. *Elife* 8:e43818.
- Blaho VA, Hla T (2014) An update on the biology of sphingosine 1-phosphate receptors. *J Lipid Res* 55:1596–1608.
- Bu S, Kapanadze B, Hsu T, Trojanowska M (2008) Opposite effects of dihydrosphingosine 1-phosphate and sphingosine 1-phosphate on transforming growth factor-beta/Smad signaling are mediated through the PTEN/PPM1A-dependent pathway. *J Biol Chem* 283:19593–19602.
- Bussolati B, Grange C, Bruno S, Buttiglieri S, Deregibus MC, Tei L, Aime S, Camussi G (2006) Neural-cell adhesion molecule (NCAM) expression by immature and tumor-derived endothelial cells favors cell organization into capillary-like structures. *Exp Cell Res* 312:913–924.
- Charpentier MS, Christine KS, Amin NM, Dorr KM, Kushner EJ, Bautch VL, Taylor JM, Conlon FL (2013) CASZ1 promotes vascular assembly and

- morphogenesis through the direct regulation of an EGFL7/RhoA-mediated pathway. *Dev Cell* 25:132–143.
- Chen D, Li L, Wang Y, Xu R, Peng S, Zhou L, Deng Z (2020) Ischemia-reperfusion injury of brain induces endothelial-mesenchymal transition and vascular fibrosis via activating let-7i/TGF- β R1 double-negative feedback loop. *FASEB J* 34:7178–7191.
- Czech B, Pfeilschifter W, Mazaheri-Omrani N, Strobel MA, Kahles T, Neumann-Haefelin T, Rami A, Huwiler A, Pfeilschifter J (2009) The immunomodulatory sphingosine 1-phosphate analog FTY720 reduces lesion size and improves neurological outcome in a mouse model of cerebral ischemia. *Biochem Biophys Res Commun* 389:251–256.
- Czupalla CJ, Liebner S, Devraj K (2014) In vitro models of the blood-brain barrier. *Methods Mol Biol* 1135:415–437.
- Devraj G, Guérit S, Seele J, Spitzer D, Macas J, Khel MI, Heidemann R, Braczynski AK, Ballhorn W, Günther S, Ogunshola OO, Mittelbronn M, Ködel U, Monoranu CM, Plate KH, Hammerschmidt S, Nau R, Devraj K, Kempf VAJ (2020) HIF-1 α is involved in blood-brain barrier dysfunction and paracellular migration of bacteria in pneumococcal meningitis. *Acta Neuropathol* 140:183–208.
- Devraj K, Klinger ME, Myers RL, Mokashi A, Hawkins RA, Simpson IA (2011) GLUT-1 glucose transporters in the blood-brain barrier: differential phosphorylation. *J Neurosci Res* 89:1913–1925.
- Fang F, Wasserman SM, Torres-Vazquez J, Weinstein B, Cao F, Li Z, Wilson KD, Yue W, Wu JC, Xie X, Pei X (2014) The role of Hath6, a newly identified shear-stress-responsive transcription factor, in endothelial cell differentiation and function. *J Cell Sci* 127:1428–1440.
- Feng S, Zou L, Wang H, He R, Liu K, Zhu H (2018) RhoA/ROCK-2 pathway inhibition and tight junction protein upregulation by catalpol suppresses lipopolysaccharide-induced disruption of blood-brain barrier permeability. *Molecules* 23:2371.
- Gao C, Qian Y, Huang J, Wang D, Su W, Wang P, Guo L, Quan W, An S, Zhang J, Jiang R (2017) A three-day consecutive fingolimod administration improves neurological functions and modulates multiple immune responses of CCI mice. *Mol Neurobiol* 54:8348–8360.
- Garcia JG, Liu F, Verin AD, Birukova A, Dechert MA, Gerthoffer WT, Bamberg JR, English D (2001) Sphingosine 1-phosphate promotes endothelial cell barrier integrity by Edg-dependent cytoskeletal rearrangement. *J Clin Invest* 108:689–701.
- Ghabriel MN, Vink R (2011) Magnesium transport across the blood-brain barriers. In: *Magnesium in the central nervous system*. Adelaide: Adelaide University Press.
- Golfier S, Kondo S, Schulze T, Takeuchi T, Vassileva G, Achtman AH, Gräler MH, Abbondanzo SJ, Wiekowski M, Kremmer E, Endo Y, Lira SA, Bacon KB, Lipp M (2010) Shaping of terminal megakaryocyte differentiation and proplatelet development by sphingosine-1-phosphate receptor S1P4. *FASEB J* 24:4701–4710.
- Gräler MH, Grosse R, Kusch A, Kremmer E, Gudermann T, Lipp M (2003) The sphingosine 1-phosphate receptor S1P4 regulates cell shape and motility via coupling to Gi and G12/13. *J Cell Biochem* 89:507–519.
- Gurnik S, Devraj K, Macas J, Yamaji M, Starke J, Scholz A, Sommer K, Di Tacchio M, Vutukuri R, Beck H, Mittelbronn M, Foerch C, Pfeilschifter W, Liebner S, Peters KG, Plate KH, Reiss Y (2016) Angiopoietin-2-induced blood-brain barrier compromise and increased stroke size are rescued by VE-PTP-dependent restoration of Tie2 signaling. *Acta Neuropathol* 131:753–773.
- He L, Vanlandewijck M, Mäe MA, Andrae J, Ando K, Del Gaudio F, Nahar K, Lebouvier T, Laviña B, Gouveia L, Sun Y, Raschperger E, Segerstolpe Å, Liu J, Gustafsson S, Räsänen M, Zarb Y, Mochizuki N, Keller A, Lendahl U, et al. (2018) Single-cell RNA sequencing of mouse brain and lung vascular and vessel-associated cell types. *Sci Data* 5:180160.
- Hla T, Venkataraman K, Michaud J (2008) The vascular S1P gradient-cellular sources and biological significance. *Biochim Biophys Acta* 1781:477–482.
- Inagaki Y, Pham TT, Fujiwara Y, Kohno T, Osborne DA, Igarashi Y, Tigyí G, Parrill AL (2005) Sphingosine 1-phosphate analogue recognition and selectivity at S1P4 within the endothelial differentiation gene family of receptors. *Biochem J* 389:187–195.
- Kakinuma N, Roy BC, Zhu Y, Wang Y, Kiyama R (2008) Kank regulates RhoA-dependent formation of actin stress fibers and cell migration via 14-3-3 in PI3K-Akt signaling. *J Cell Biol* 181:537–549.
- Kang Y, Wang F, Feng J, Yang D, Yang X, Yan X (2006) Knockdown of CD146 reduces the migration and proliferation of human endothelial cells. *Cell Res* 16:313–318.
- Keistner R-I, Mayser F, Vutukuri R, Hansen L, Günther S, Brunkhorst R, Devraj K, Pfeilschifter W (2020) Gene expression dynamics at the neurovascular unit during early regeneration after cerebral ischemia/reperfusion injury in mice. *Front Neurosci* 14:280.
- Kim GS, Yang L, Zhang G, Zhao H, Selim M, McCullough LD, Kluk MJ, Sanchez T (2015) Critical role of sphingosine-1-phosphate receptor-2 in the disruption of cerebrovascular integrity in experimental stroke. *Nat Commun* 6:7893.
- Kim J, Kim Y, Kim HT, Kim DW, Ha Y, Kim J, Kim CH, Lee I, Song K (2009) TC1(C8orf4) is a novel endothelial inflammatory regulator enhancing NF-kappaB activity. *J Immunol* 183:3996–4002.
- Kraan J, van den Broek P, Verhoef C, Grunhagen DJ, Taal W, Gratama JW, Sleijfer S (2014) Endothelial CD276 (B7-H3) expression is increased in human malignancies and distinguishes between normal and tumour-derived circulating endothelial cells. *Br J Cancer* 111:149–156.
- Li J, Ballif BA, Powelka AM, Dai J, Gygi SP, Hsu VW (2005) Phosphorylation of ACAP1 by Akt regulates the stimulation-dependent recycling of integrin beta1 to control cell migration. *Dev Cell* 9:663–673.
- Liao Y, Smyth GK, Shi W (2014) featureCounts: an efficient general purpose program for assigning sequence reads to genomic features. *Bioinformatics* 30:923–930.
- Love MI, Huber W, Anders S (2014) Moderated estimation of fold change and dispersion for RNA-seq data with DESeq2. *Genome Biol* 15:550.
- Lycck R, Ruderisch N, Moll AG, Steiner O, Cohen CD, Engelhardt B, Makrides V, Verrey F (2009) Culture-induced changes in blood-brain barrier transcriptome: implications for amino-acid transporters in vivo. *J Cereb Blood Flow Metab* 29:1491–1502.
- Ma J, Sanchez-Duffhues G, Goumans M-J, ten Dijke P (2020) TGF- β -induced endothelial to mesenchymal transition in disease and tissue engineering. *Front Cell Dev Biol* 8:260.
- Matloubian M, Lo CG, Cinamon G, Lesneski MJ, Xu Y, Brinkmann V, Allende ML, Proia RL, Cyster JG (2004) Lymphocyte egress from thymus and peripheral lymphoid organs is dependent on S1P receptor 1. *Nature* 427:355–360.
- Mukherjee J, DeSouza LV, Micallef J, Karim Z, Croul S, Siu KWM, Guha A (2009) Loss of collapsin response mediator Protein1, as detected by iTRAQ analysis, promotes invasion of human gliomas expressing mutant EGFRvIII. *Cancer Res* 69:8545–8554.
- Nibbs RJB, Graham GJ (2013) Immune regulation by atypical chemokine receptors. *Nat Rev Immunol* 13:815–829.
- Nitzsche A, Poitvin M, Benarab A, Bonnin P, Faraco G, Uchida H, Favre J, Garcia-Bonilla L, Garcia MCL, Léger PL, Théron P, Mathivet T, Autret G, Baudrie V, Couty L, Kono M, Chevallier A, Niazi H, Tharaux PL, Chun J, et al. (2021) Endothelial S1P1 signaling counteracts infarct expansion in ischemic stroke. *Circ Res* 128:363–382.
- Ohotski J, Rosen H, Bittman R, Pyne S, Pyne NJ (2014) Sphingosine kinase 2 prevents the nuclear translocation of sphingosine 1-phosphate receptor-2 and tyrosine 416 phosphorylated c-Src and increases estrogen receptor negative MDA-MB-231 breast cancer cell growth: the role of sphingosine 1-phosphate receptor-4. *Cell Signal* 26:1040–1047.
- Olesch C, Sirait-Fischer E, Berkefeld M, Fink AF, Susen RM, Ritter B, Michels BE, Steinhilber D, Greten FR, Savai R, Takeda K, Brüne B, Weigert A (2020) S1PR4 ablation reduces tumor growth and improves chemotherapy via CD8+ T cell expansion. *J Clin Invest* 130:5461–5476.
- Park SJ, Im DS (2019) Deficiency of sphingosine-1-phosphate receptor 2 (S1P2) attenuates bleomycin-induced pulmonary fibrosis. *Biomol Ther (Seoul)* 27:318–326.
- Perry HM, Huang L, Ye H, Liu C, Sung SSJ, Lynch KR, Rosin DL, Bajwa A, Okusa MD (2016) Endothelial sphingosine 1-phosphate receptor-1 mediates protection and recovery from acute kidney injury. *J Am Soc Nephrol* 27:3383–3393.
- Pfeilschifter W, Bohmann F, Baumgarten P, Mittelbronn M, Pfeilschifter J, Lindhoff-Last E, Steinmetz H, Foerch C (2012) Thrombolysis with recombinant tissue plasminogen activator under dabigatran anticoagulation in experimental stroke. *Ann Neurol* 71:624–633.
- Reinhard NR, Mastop M, Yin T, Wu Y, Bosma EK, Gadella TWJ, Goedhart J, Hordijk PL (2017) The balance between Gai-Cdc42/Rac and Ga12/13-RhoA pathways determines endothelial barrier regulation by sphingosine-1-phosphate. *Mol Biol Cell* 28:3371–3382.
- Salas-Perdomo A, Miró-Mur F, Gallizioli M, Brait VH, Justicia C, Meissner A, Urra X, Chamorro A, Planas AM (2019) Role of the S1P pathway and

- inhibition by fingolimod in preventing hemorrhagic transformation after stroke. *Sci Rep* 9:8309.
- Sanchez T, Skoura A, Wu MT, Casserly B, Harrington EO, Hla T (2007) Induction of vascular permeability by the sphingosine-1-phosphate receptor-2 (S1P2R) and its downstream effectors ROCK and PTEN. *Arterioscler Thromb Vasc Biol* 27:1312–1318.
- Sánchez del Pino MM, Hawkins RA, Peterson DR (1995) Biochemical discrimination between luminal and abluminal enzyme and transport activities of the blood-brain barrier. *J Biol Chem* 270:14907–14912.
- Schwab SR, Pereira JP, Matloubian M, Xu Y, Huang Y, Cyster JG (2005) Lymphocyte sequestration through S1P lyase inhibition and disruption of S1P gradients. *Science* 309:1735–1739.
- Simpson IA, Vannucci SJ, DeJoseph MR, Hawkins RA (2001) Glucose transporter asymmetries in the bovine blood-brain barrier. *J Biol Chem* 276:12725–12729.
- Singleton PA, Dudek SM, Chiang ET, Garcia JGN (2005) Regulation of sphingosine 1-phosphate-induced endothelial cytoskeletal rearrangement and barrier enhancement by S1P1 receptor, PI3 kinase, Tiam1/Rac1, and alpha-actinin. *FASEB J* 19:1646–1656.
- Sørensen-Zender I, Chen R, Rong S, David S, Melk A, Haller H, Schmitt R (2019) Binding to carboxypeptidase M mediates protective effects of fibrinopeptide B β 15–42. *Transl Res* 213:124–135.
- Stenmark KR, Frid M, Perros F (2016) Endothelial-to-mesenchymal transition: an evolving paradigm and a promising therapeutic target in PAH. *Circulation* 133:1734–1737.
- Su F, Li B, Wang J, Xu X, Ren R, Li L, Gao F, Liu X (2009) Molecular regulation of vasculogenic mimicry in human uveal melanoma cells: role of helix-loop-helix Id2 (inhibitor of DNA binding 2). *Graefes Arch Clin Exp Ophthalmol* 247:411–419.
- Takuwa Y, Ikeda H, Okamoto Y, Takuwa N, Yoshioka K (2013) Sphingosine-1-phosphate as a mediator involved in development of fibrotic diseases. *Biochim Biophys Acta* 1831:185–192.
- Trexler M, Bányai L, Patthy L (2001) A human protein containing multiple types of protease-inhibitory modules. *Proc Natl Acad Sci USA* 98:3705–3709.
- van Doorn R, Lopes Pinheiro MA, Kooij G, Lakeman K, van het Hof B, van der Pol SMA, Geerts D, van Horsen J, van der Valk P, van der Kam E, Ronken E, Reijerkerk A, de Vries HE (2012) Sphingosine 1-phosphate receptor 5 mediates the immune quiescence of the human brain endothelial barrier. *J Neuroinflammation* 9:133.
- Vanlandewijck M, He L, Mäe MA, Andrae J, Ando K, Del Gaudio F, Nahar K, Lebouvier T, Laviña B, Gouveia L, Sun Y, Raschperger E, Räsänen M, Zarb Y, Mochizuki N, Keller A, Lendahl U, Betsholtz C (2018) A molecular atlas of cell types and zonation in the brain vasculature. *Nature* 554:475–480.
- Vanoye CG, Kunic JD, Ehring GR, George AL (2013) Mechanism of sodium channel NaV1.9 potentiation by G-protein signaling. *J Gen Physiol* 141:193–202.
- Vutukuri R, Brunkhorst R, Kestner R-I, Hansen L, Bouzas NF, Pfeilschifter J, Devraj K, Pfeilschifter W (2018) Alteration of sphingolipid metabolism as a putative mechanism underlying LPS-induced BBB disruption. *J Neurochem* 144:172–185.
- Wägsäter D, Björk H, Zhu C, Björkegren J, Valen G, Hamsten A, Eriksson P (2008) ADAMTS-4 and -8 are inflammatory regulated enzymes expressed in macrophage-rich areas of human atherosclerotic plaques. *Atherosclerosis* 196:514–522.
- Wu Y, Deng J, Rychahou PG, Qiu S, Evers BM, Zhou BP (2009) Stabilization of snail by NF-kappaB is required for inflammation-induced cell migration and invasion. *Cancer Cell* 15:416–428.
- Wulff H, Castle NA (2010) Therapeutic potential of KCa3.1 blockers: recent advances and promising trends. *Expert Rev Clin Pharmacol* 3:385–396.
- Xin C, Ren S, Kleuser B, Shabahang S, Eberhardt W, Radeke H, Schäfer-Korting M, Pfeilschifter J, Huwiler A (2004) Sphingosine 1-phosphate cross-activates the Smad signaling cascade and mimics transforming growth factor-beta-induced cell responses. *J Biol Chem* 279:35255–35262.
- Zhang W, An J, Jawadi H, Siow DL, Lee J-F, Zhao J, Gartung A, Maddipati KR, Honn KV, Wattenberg BW, Lee MJ (2013) Sphingosine-1-phosphate receptor-2 mediated NF κ B activation contributes to tumor necrosis factor- α induced VCAM-1 and ICAM-1 expression in endothelial cells. *Prostaglandins Other Lipid Mediat* 106:62–71.
- Zhang Y, Zhang XF, Fleming MR, Amiri A, El-Hassar L, Surguchev AA, Hyland C, Jenkins DP, Desai R, Brown MR, Gazula VR, Waters MF, Large CH, Horvath TL, Navaratnam D, Vaccarino FM, Forscher P, Kaczmarek LK (2016) Kv3.3 channels bind Hax-1 and Arp2/3 to assemble a stable local actin network that regulates channel gating. *Cell* 165:434–448.